NASA TECHNICAL MEMORANDUM

NASA TM X-1771

NASA TM X-1771

ANTENNA EFFECTS ON THE AERODYNAMIC CHARACTERISTICS OF A 0.410-SCALE MODEL OF THE CAJUN ROCKET AT MACH NUMBERS FROM 2.30 TO 4.63

by Lloyd S. Jernell

Langley Research Center
Langley Station, Hampton, Va.

NATIONAL AERONAUTICS AND SPACE ADMINISTRATION • WASHINGTON, D. C. • MARCH 1969

NASA TM X-1771

ANTENNA EFFECTS ON THE AERODYNAMIC CHARACTERISTICS OF A 0.410-SCALE MODEL OF THE CAJUN ROCKET AT MACH NUMBERS FROM 2.30 TO 4.63

By Lloyd S. Jernell

Langley Research Center
Langley Station, Hampton, Va.

NATIONAL AERONAUTICS AND SPACE ADMINISTRATION

For sale by the Clearinghouse for Federal Scientific and Technical Information
Springfield, Virginia 22151 – CFSTI price $3.00

Page Intentionally Left Blank

ANTENNA EFFECTS ON THE AERODYNAMIC CHARACTERISTICS OF A 0.410-SCALE MODEL OF THE CAJUN ROCKET AT MACH NUMBERS FROM 2.30 TO 4.63

By Lloyd S. Jernell
Langley Research Center

SUMMARY

The effects of several proposed antenna configurations on the aerodynamic characteristics of a 0.410-scale model of the Cajun rocket have been investigated in the Langley Unitary Plan wind tunnel at Mach numbers from 2.30 to 4.63. Data were obtained at angles of attack to approximately 12° for roll angles of 0°, 22.5°, and 45°.

The results indicate that the antenna configurations investigated have no significant effects on either the normal-force or pitching-moment parameters. The turnstile and Dovap antennas contribute appreciably to the axial-force coefficient. The greater values of the induced lateral characteristics are generally produced by the quadraloop and Dovap antennas.

INTRODUCTION

The Nike-Cajun rocket is a two-stage solid-propellant unguided vehicle designed primarily as a meteorological sounding-rocket system. The effects of several proposed antenna configurations on the aerodynamic characteristics of the second-stage (Cajun) vehicle have been investigated in the Langley Unitary Plan wind tunnel at Mach numbers from 2.30 to 4.63. Data were obtained at angles of attack to approximately 12° for roll angles of 0°, 22.5°, and 45°. The test Reynolds number was 2.0×10^{6} per foot (6.56×10^{6} per meter).

The results of tests to determine the aerodynamic characteristics of a spinning and nonspinning model of a similar Cajun configuration are reported in reference 1.

SYMBOLS

The data are referred to the nonrolling body-axis system. The location of the reference moment center is shown in figure 1. The symbols are defined as follows:

A	body cross-sectional area, 0.0388 foot^2 (0.00360 meter^2)
C_A	axial-force coefficient, $\frac{\text{Axial force}}{qA}$
$C_{A,o}$	axial-force coefficient at $\alpha = 0^o$
C_l	rolling-moment coefficient, $\frac{\text{Rolling moment}}{qAd}$
$C_{l,i}$	induced rolling-moment coefficient, $C_l - \left(C_l\right)_{\phi=0}$
C_m	pitching-moment coefficient, $\frac{\text{Pitching moment}}{qAd}$
C_{m_α}	slope of pitching-moment curve ($\alpha \approx 0$), $\frac{\partial C_m}{\partial \alpha}$
C_N	normal-force coefficient, $\frac{\text{Normal force}}{qA}$
C_{N_α}	slope of normal-force curve ($\alpha \approx 0$), $\frac{\partial C_N}{\partial \alpha}$
C_n	yawing-moment coefficient, $\frac{\text{Yawing moment}}{qAd}$
$C_{n,i}$	induced yawing-moment coefficient, $C_n - \left(C_n\right)_{\phi=0}$
C_Y	side-force coefficient, $\frac{\text{Side force}}{qA}$
$C_{Y,i}$	induced side-force coefficient, $C_Y - \left(C_Y\right)_{\phi=0}$
d	body diameter, 2.668 inches (6.777 centimeters)
l	length of model, measured from theoretical nose apex, inches (centimeters)
M	Mach number
q	dynamic pressure, pounds/foot^2 (newtons/meter^2)
x_{ac}	location of aerodynamic center from theoretical nose apex, $x_{mc} - \frac{C_{m_\alpha}}{C_{N_\alpha}} d$, inches (centimeters)

x_{mc} location of moment center from theoretical nose apex, inches (centimeters)

α angle of attack referred to model center line, degrees

ϕ angle of roll (positive for right roll), degrees

APPARATUS AND METHODS

Models

Details of the 0.410-scale model are provided in the drawings of figure 1. The model consisted of a basic body, fins, and various arrangements of detachable antennas. A 7°-wedge roll-control tab was provided at the trailing edge of each fin to produce a negative rolling moment. (See fig. 1(b).) Four Dovap antennas were located at 90° intervals around the body. (See figs. 1(a) and 1(c).) Two quadraloop antennas, one on each side of the body, were provided for both a forward and rearward location. (See figs. 1(a) and 1(d).) Also investigated were four turnstile antennas located at 90° intervals around the body. (See figs. 1(a) and 1(e).)

Tunnel

The investigation was performed in the high Mach number test section of the Langley Unitary Plan wind tunnel, which is a variable-pressure, continuous-flow facility. The test section is approximately 4 feet (1.22 meters) square and 7 feet (2.13 meters) in length. The nozzle leading to the test section is of the asymmetric sliding-block type which permits a continuous variation in Mach number from about 2.3 to 4.7.

Measurements, Corrections, and Tests

Aerodynamic forces and moments were measured by means of a sting-supported six-component electrical-strain-gage balance housed within the model. The tests were conducted at Mach numbers of 2.30, 2.96, 3.95, and 4.63 and at a Reynolds number of 2.0×10^6 per foot (6.56×10^6 per meter). The angle-of-attack range was from about -4° to 12° for roll angles of 0°, 22.5°, and 45°. The angles of attack were corrected for tunnel flow angularity and for deflection of the balance and sting due to aerodynamic load. The axial-force coefficient has been adjusted to a condition of free-stream static pressure at the model base. The stagnation dewpoint was maintained below -30° F (230° K) to avoid moisture condensation effects. A 0.06-inch-width (0.15-cm) transition strip composed of No. 60 sand was affixed around the nose 1.2 inches (3.05 cm) aft of the nose apex.

DISCUSSION

The basic longitudinal aerodynamic characteristics are presented in figures 2 to 6. These data show an increase in the normal-force-coefficient slope with increase in angle of attack, which is characteristic of this type of vehicle in the test Mach number range. Although the pitching-moment data generally exhibit a linear variation with angle of attack, an exception is the configuration employing turnstile antennas, in which case a small degree of nonlinearity exists at the lower angles of attack and higher Mach numbers. A summary of the longitudinal stability characteristics (fig. 7) indicates that as Mach number is increased, all configurations exhibit increases in C_{m_α} (that is, C_{m_α} becomes less negative). There is a forward movement of the aerodynamic center as Mach number is increased. Throughout the Mach number range, the addition of either the Dovap or quadraloop antennas results in a forward movement of the aerodynamic center, whereas the addition of turnstile antennas produces a slightly rearward shift.

All configurations exhibit a decrease in $C_{A,o}$, the axial-force coefficient at $\alpha = 0^o$, as Mach number is increased. (See fig. 8.) Only a slight increase in $C_{A,o}$ is noted with the addition of quadraloop antennas; however, a significant increase occurs with the addition of either the Dovap or turnstile antennas.

The basic lateral aerodynamic characteristics are presented in figures 9 to 13 and are summarized in figures 14 to 16 in terms of the induced effects due to model roll. The basic configuration (no antennas) exhibits induced lateral effects at the higher angles of attack, particularly at $\phi = 22.5^o$. These effects diminish somewhat with increase in Mach number. The higher values of induced roll are generally produced by the Dovap and forward quadraloop antennas, the effects of the Dovap occurring mainly at $\phi = 22.5^o$. The forward quadraloop antennas produce large values of induced roll at $\phi = 22.5^o$ and $\phi = 45^o$; however, the effects are considerably reduced with increase in Mach number. The largest values of induced yaw occur in conjunction with the Dovap antennas at the higher test Mach numbers and angles of attack.

CONCLUSIONS

Results of tests on a 0.410-scale model of the Cajun sounding rocket with various antenna configurations at Mach numbers from 2.30 to 4.63 indicate the following conclusions:

1. The antenna configurations investigated have no significant effects on either the normal-force or pitching-moment parameters.

2. The turnstile and Dovap antennas contribute appreciably to the axial-force coefficient.

3. The greater values of induced lateral characteristics are generally produced by the quadraloop and Dovap antennas.

Langley Research Center,
National Aeronautics and Space Administration,
Langley Station, Hampton, Va., February 6, 1969,
124-07-05-01-23.

REFERENCE

1. Falanga, Ralph A.: Supersonic Investigation of a Spinning and Nonspinning Model of a Cajun (or Apache) Rocket Vehicle With Roll-Control Tabs. NASA TN D-2576, 1965.

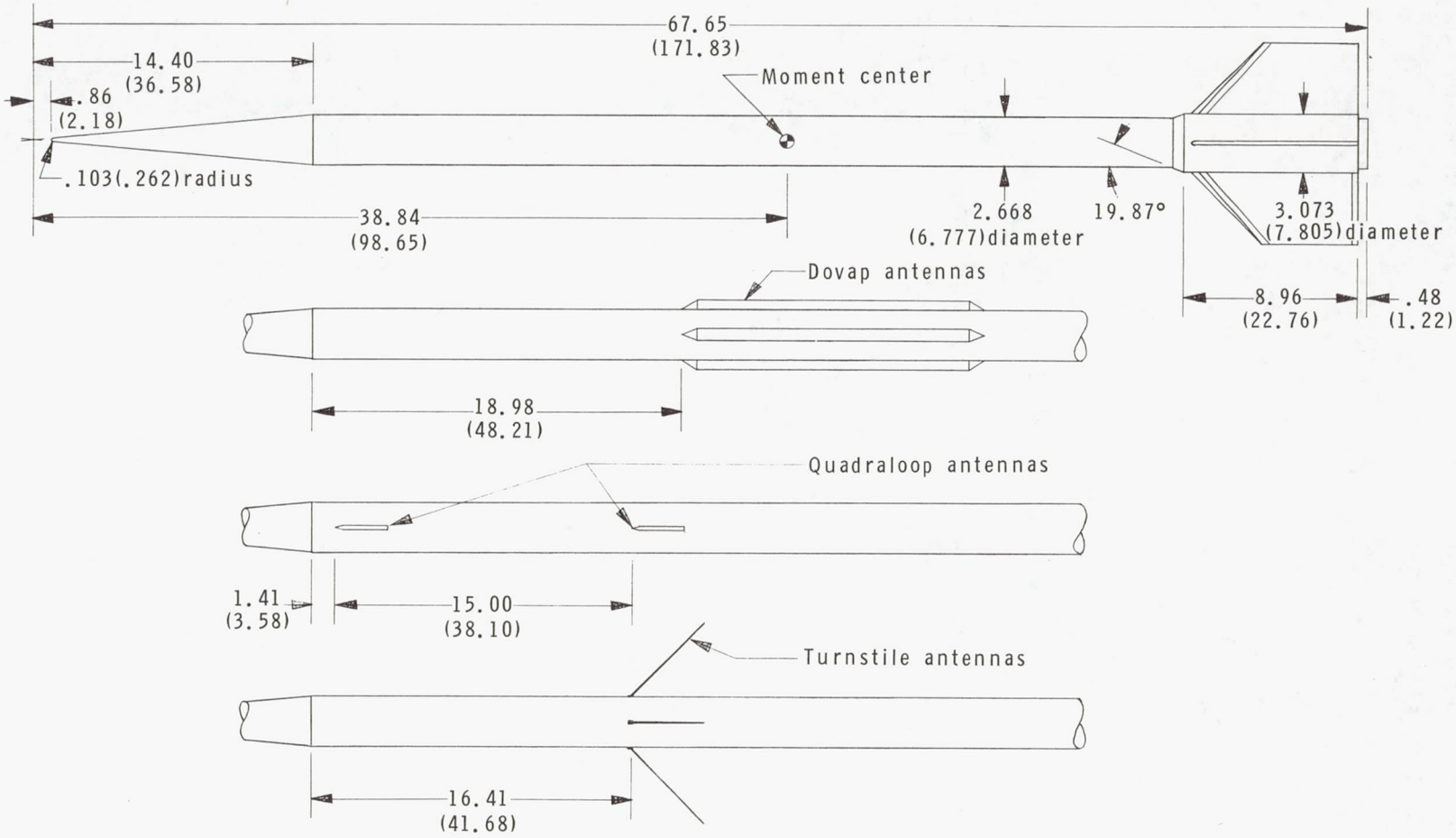

(a) Clean configuration and location of antennas.

Figure 1.- Drawings of 0.410-scale model of Cajun rocket. (Linear dimensions are given in inches and parenthetically in centimeters.)

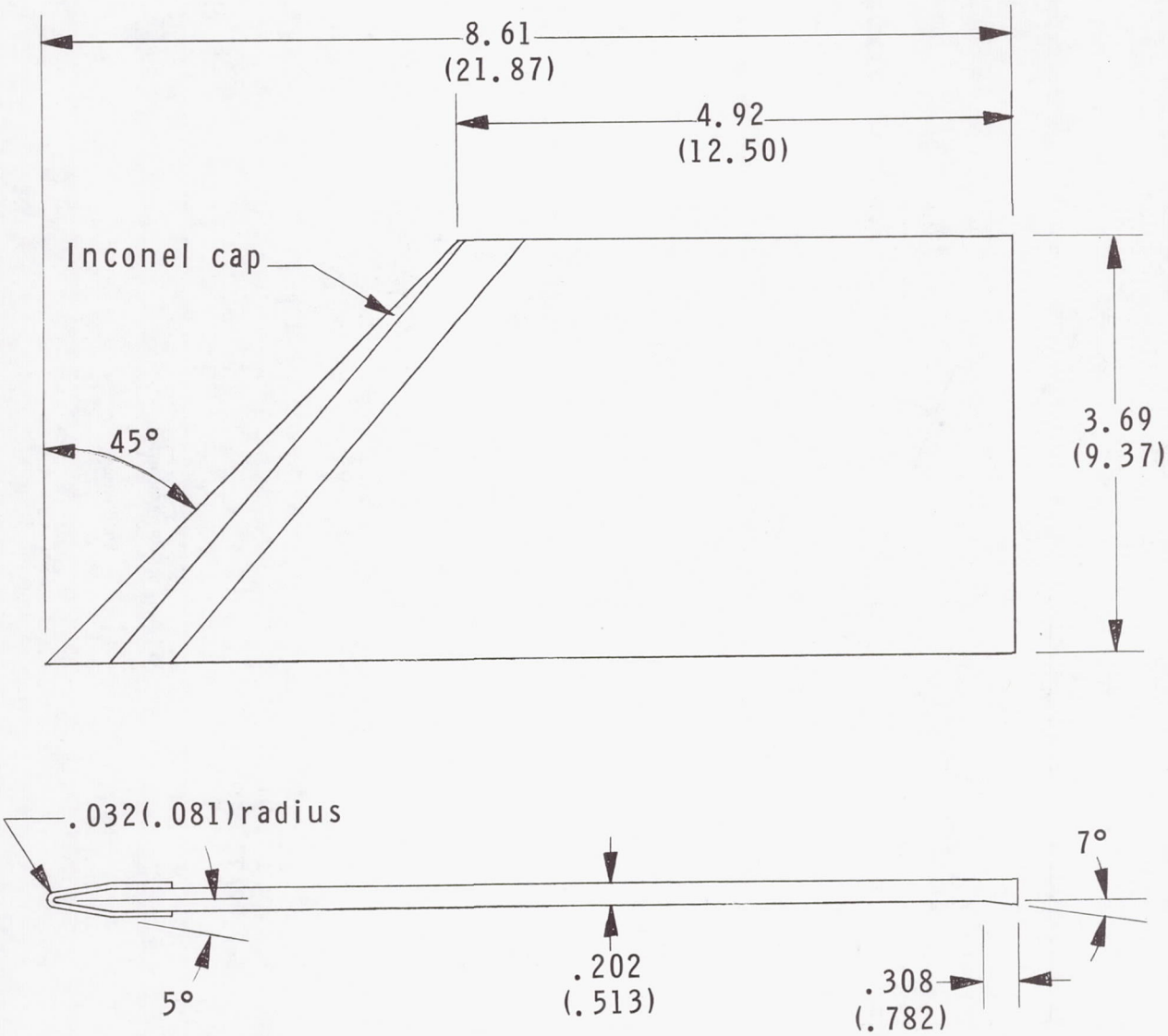

(b) Fin details.

Figure 1.- Continued.

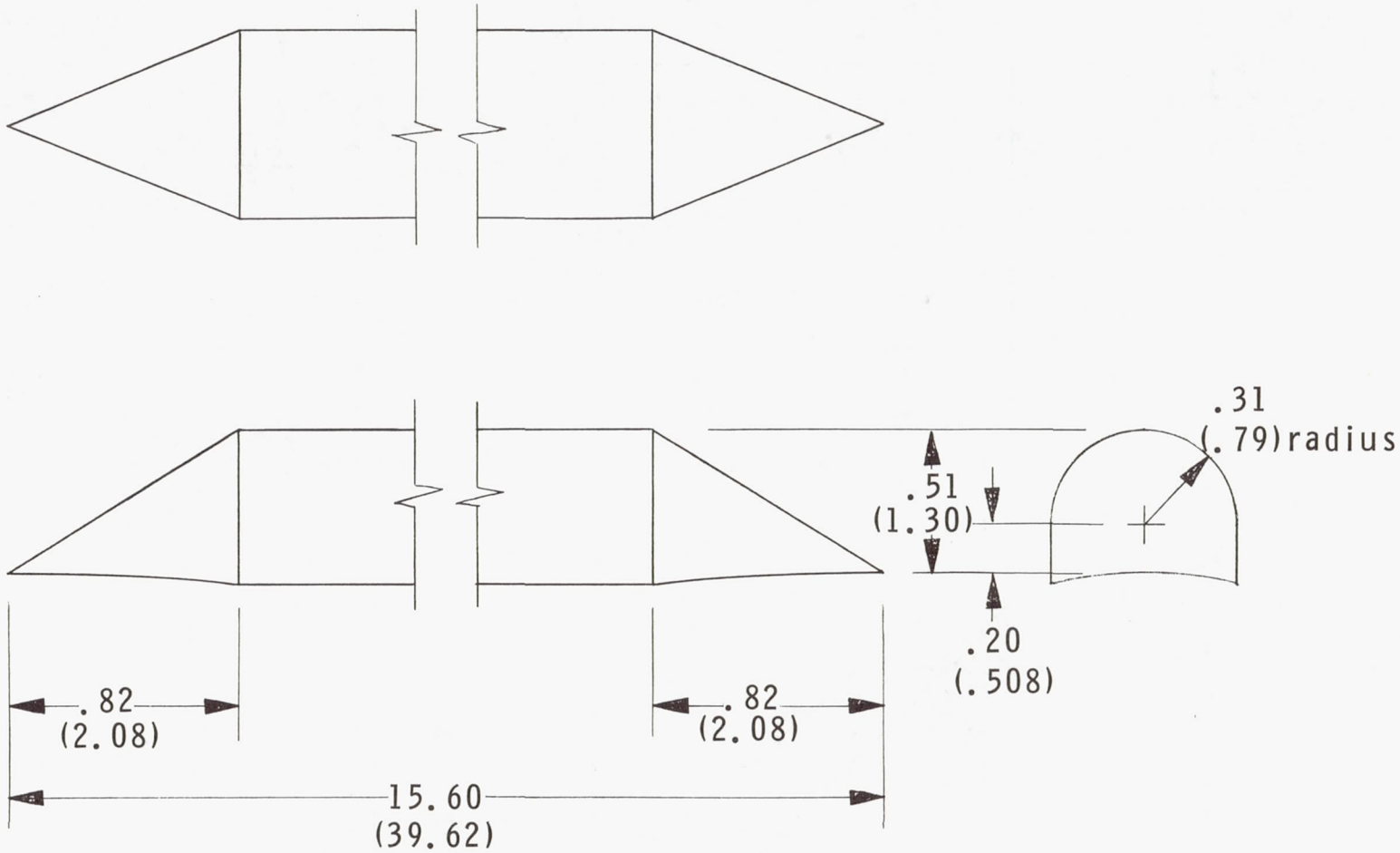

(c) Details of Dovap antennas.

Figure 1.- Continued.

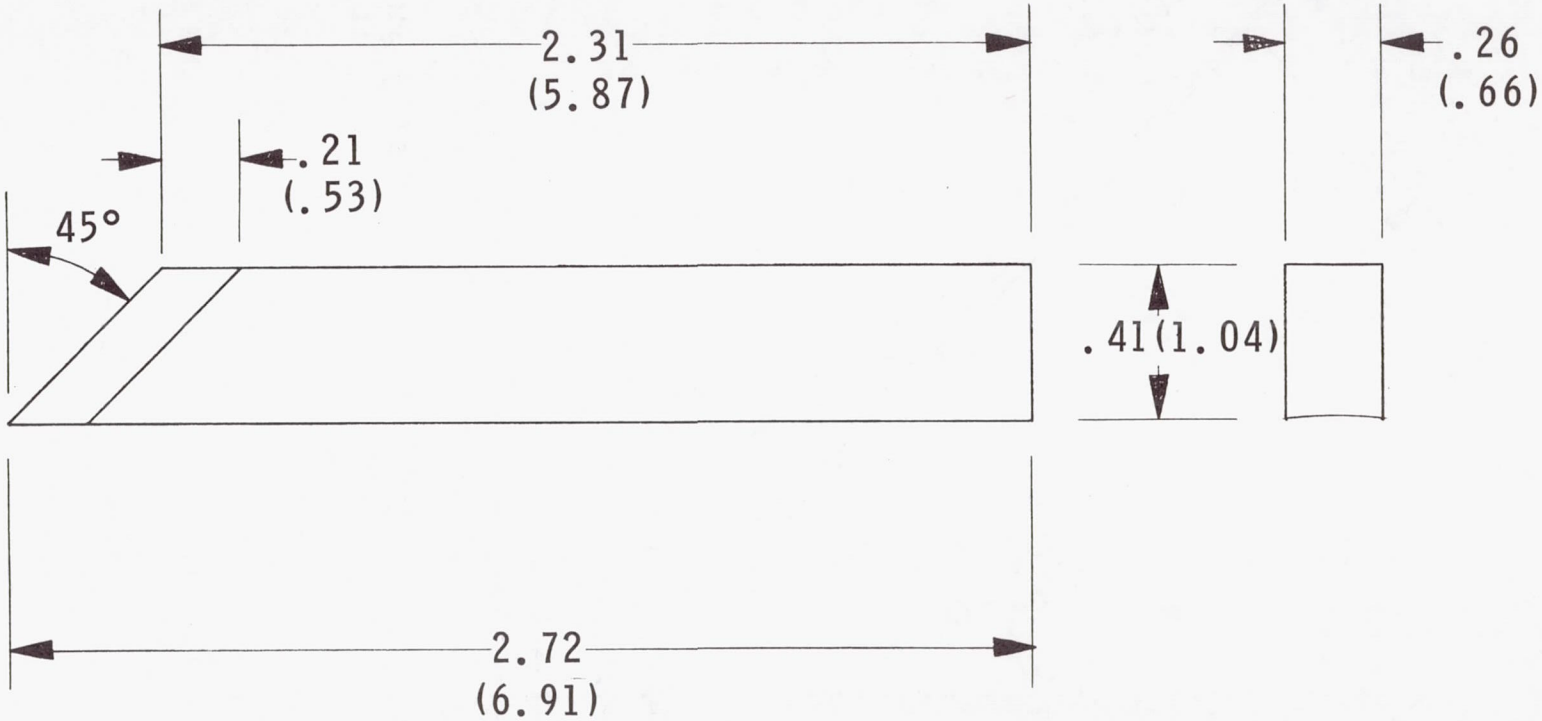

(d) Details of quadraloop antennas.

Figure 1.- Continued.

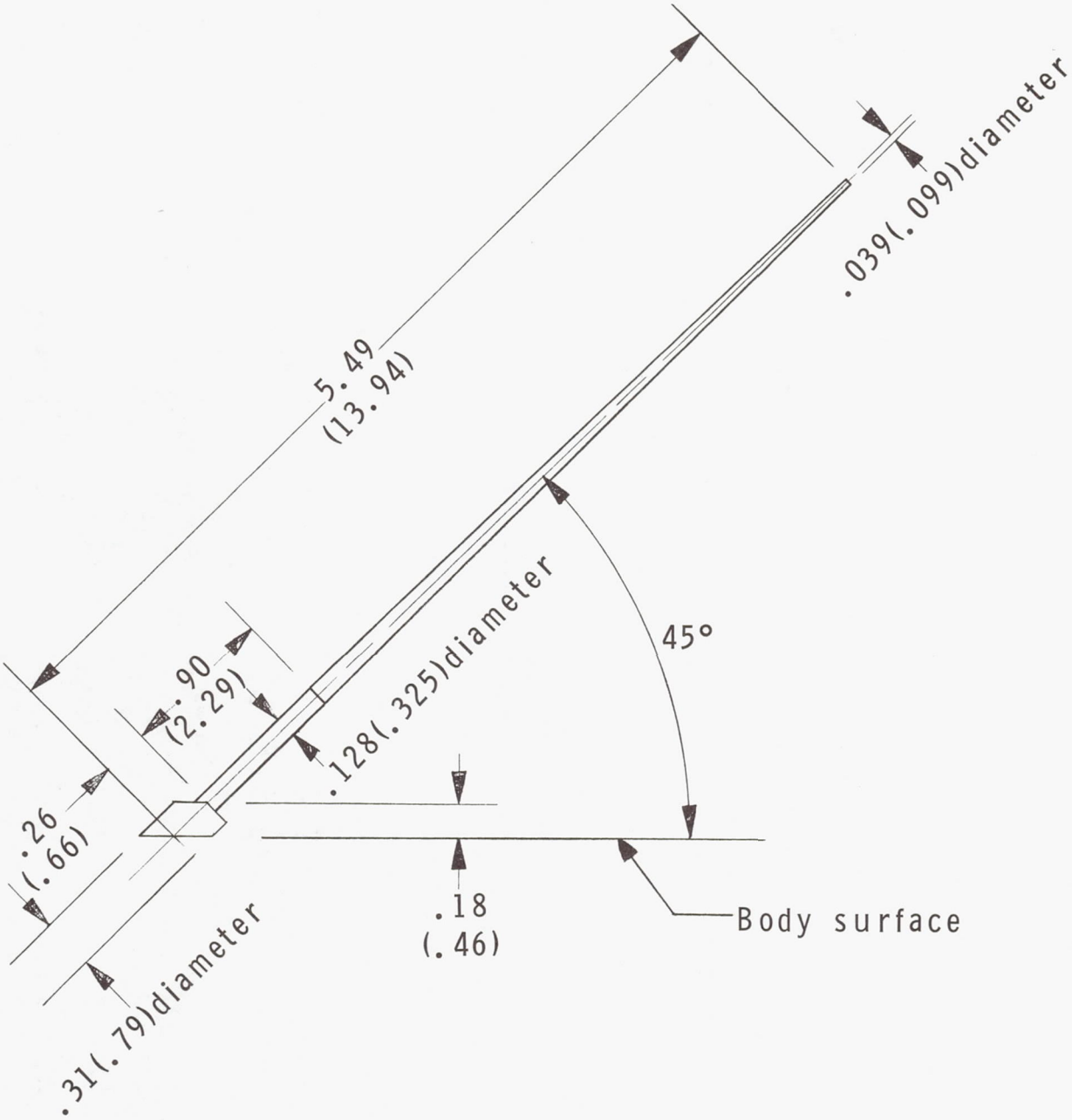

(e) Details of turnstile antennas.

Figure 1.- Concluded.

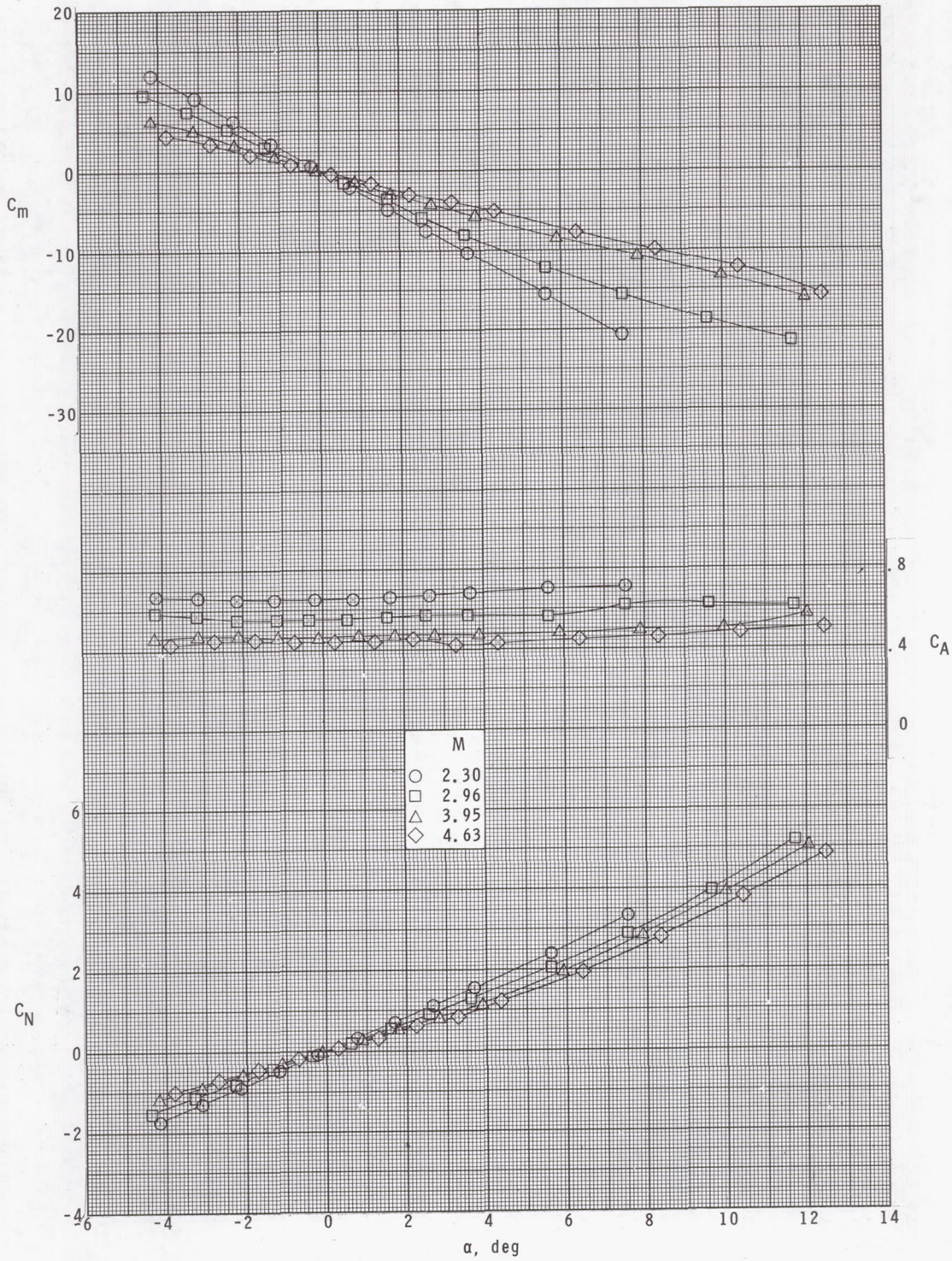

(a) $\Phi = 0^0$.

Figure 2.- Longitudinal aerodynamic characteristics of clean configuration (no antennas).

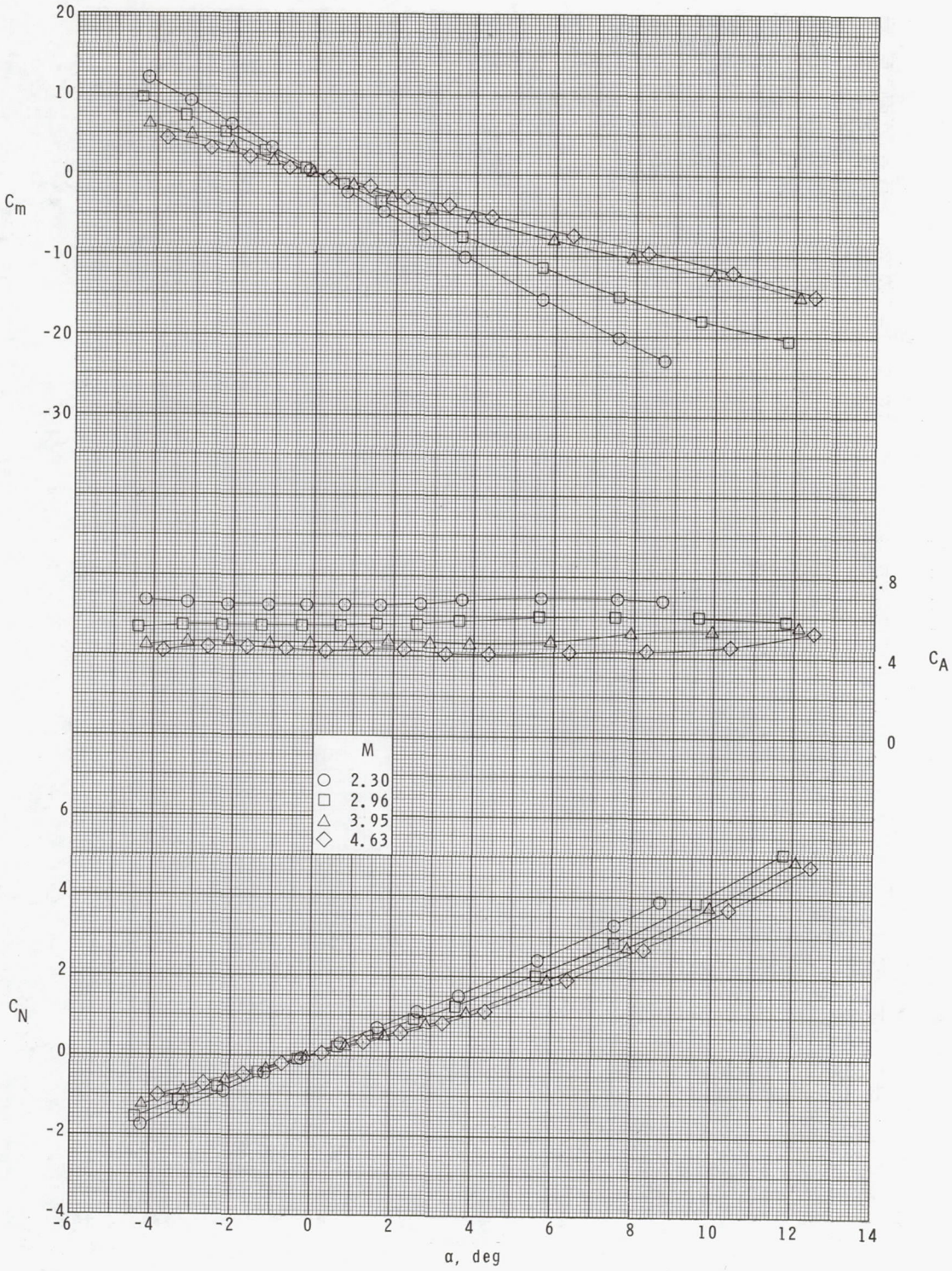

(b) $\Phi = 22.5^{0}$.

Figure 2.- Continued.

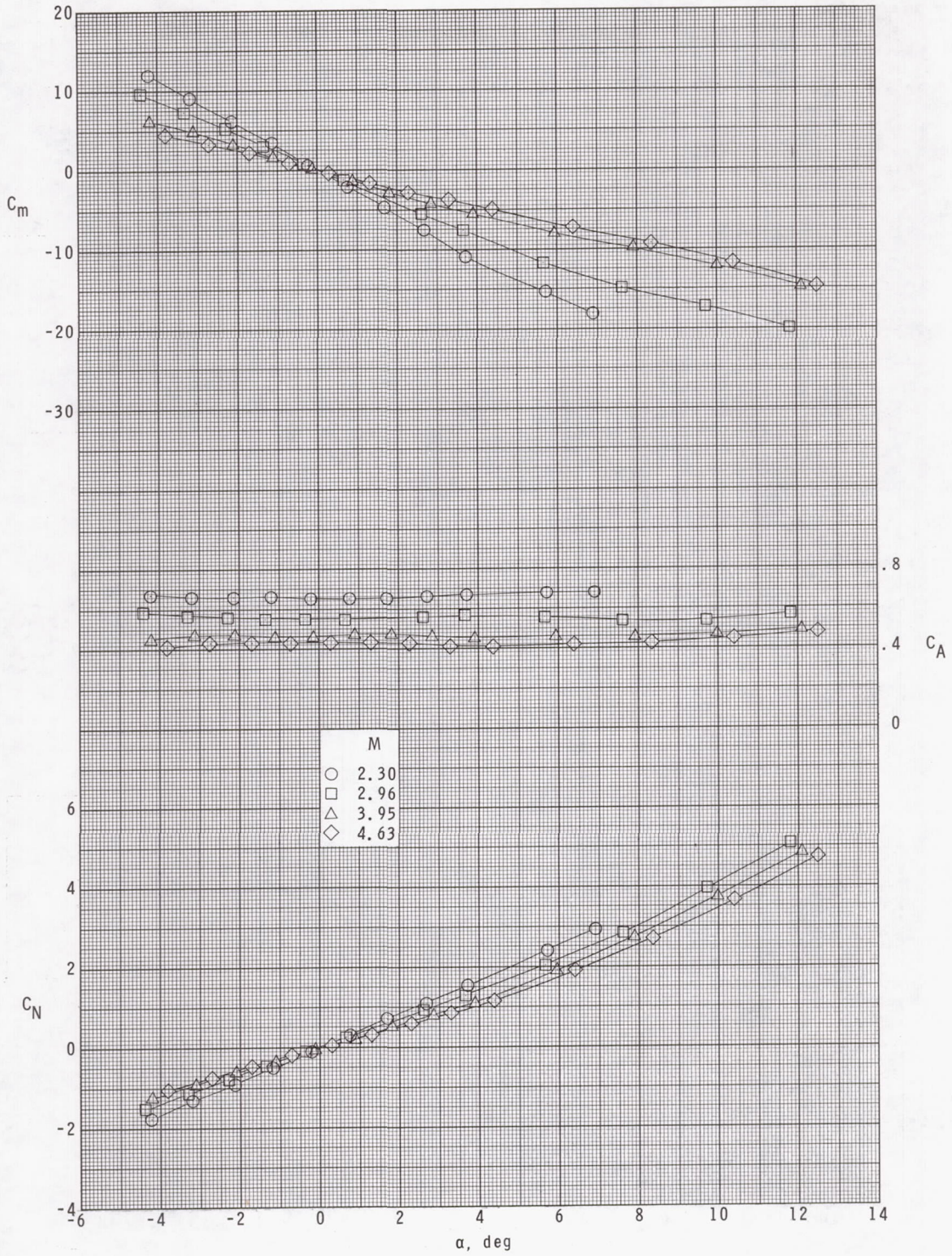

(c) $\Phi = 45^{\circ}$.

Figure 2.- Concluded.

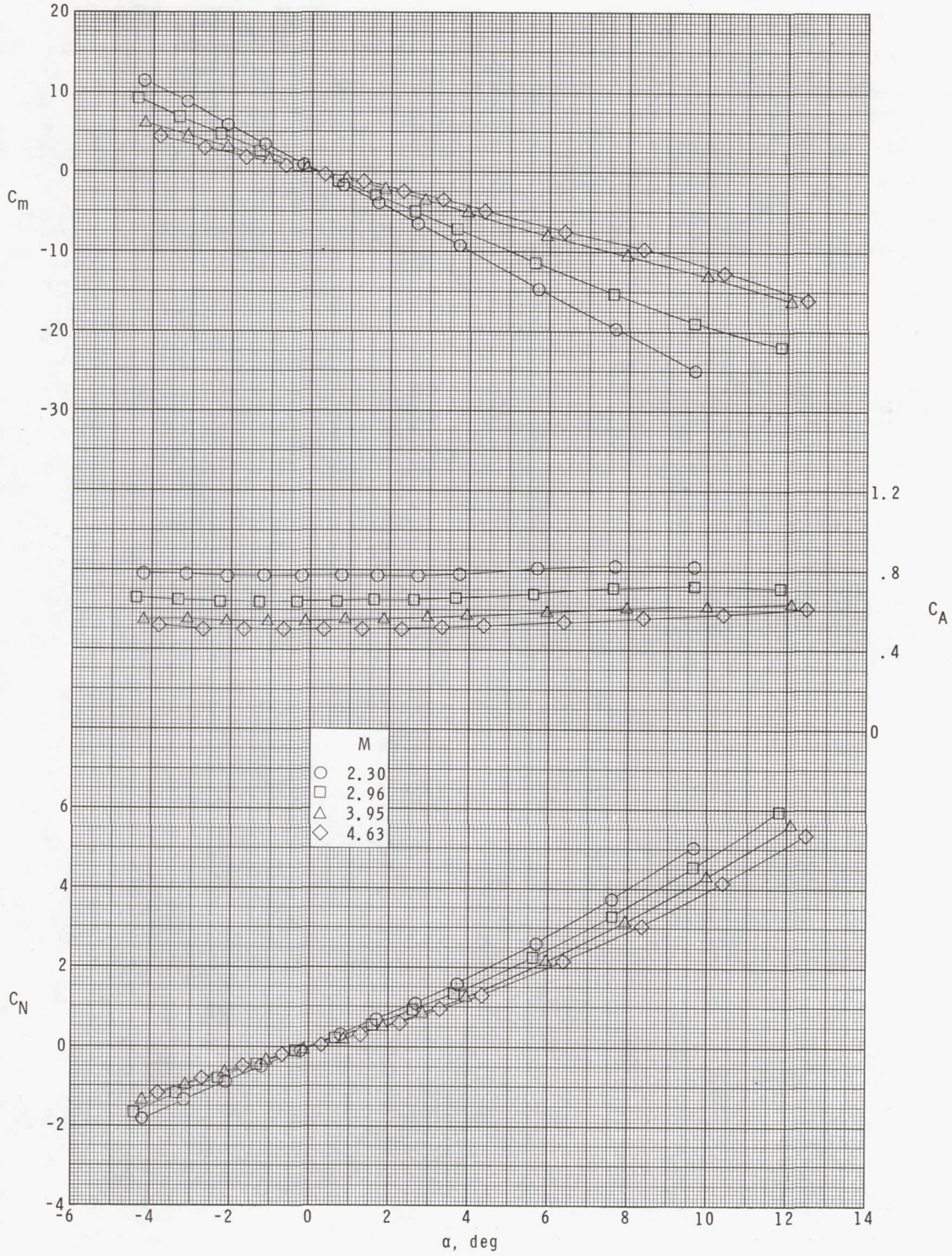

(a) $\Phi = 0^{\circ}$.

Figure 3.- Longitudinal aerodynamic characteristics of model with Dovap antennas.

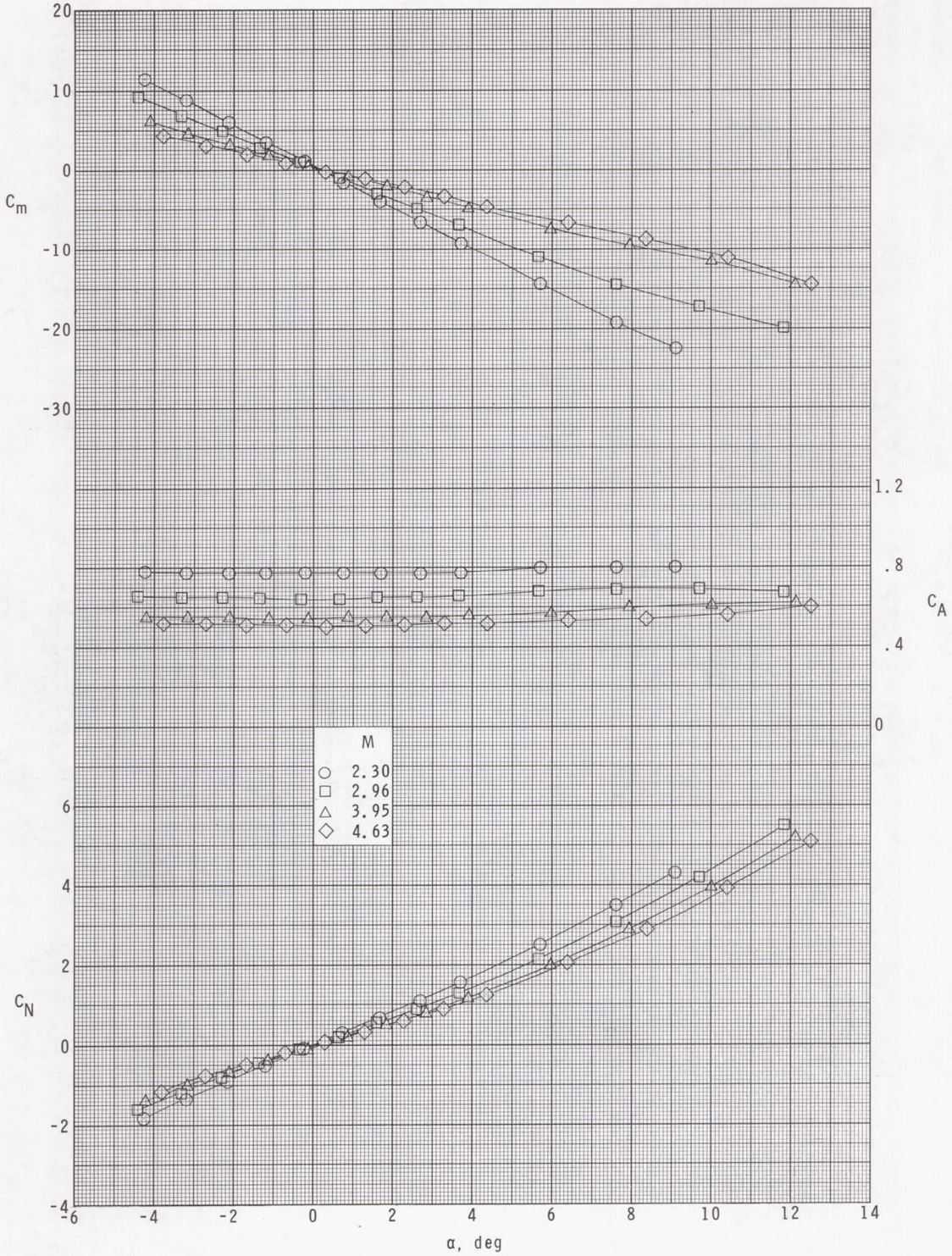

(b) $\Phi = 22.5^{\circ}$.

Figure 3.- Continued.

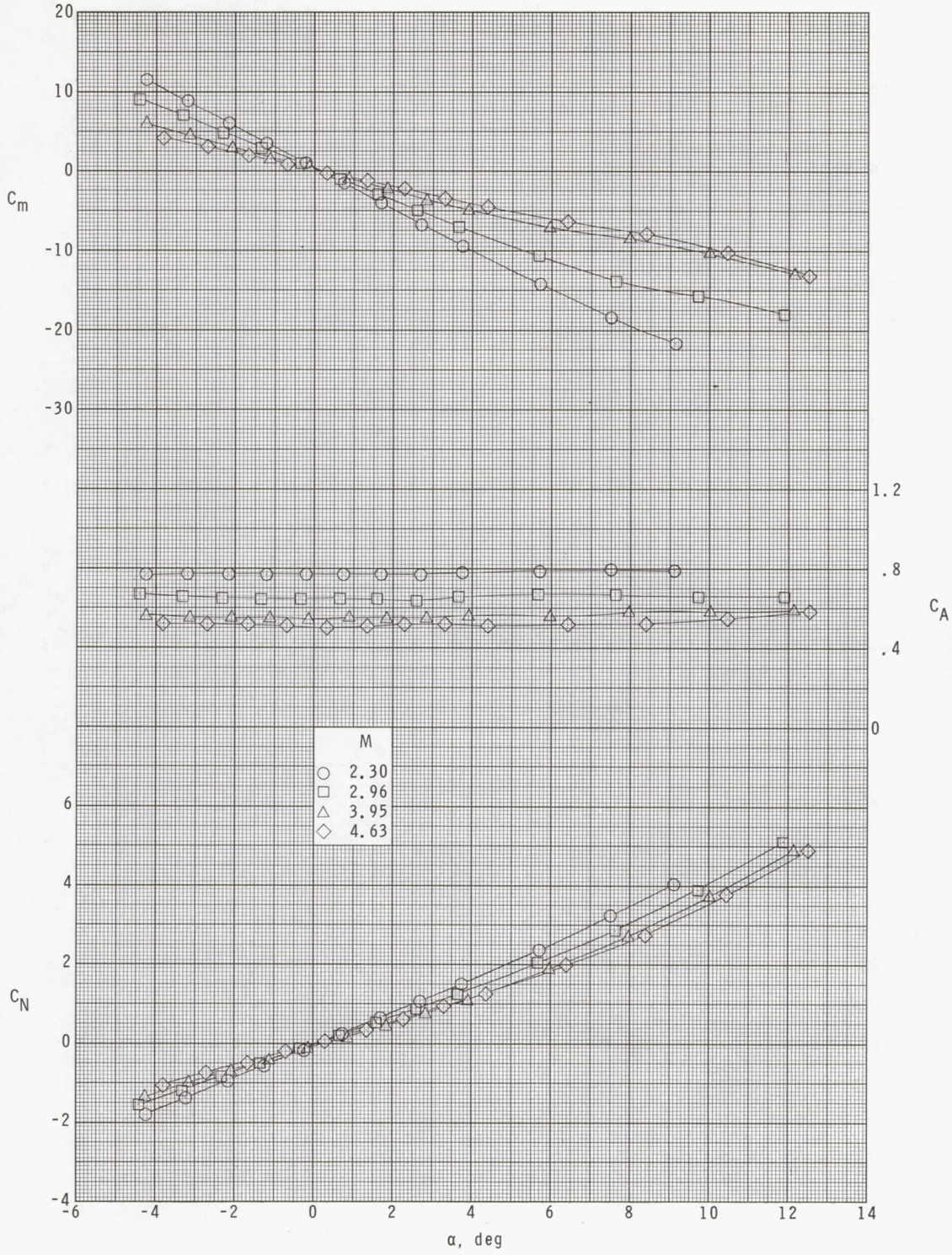

(c) $\Phi = 45^{\circ}$.

Figure 3.- Concluded.

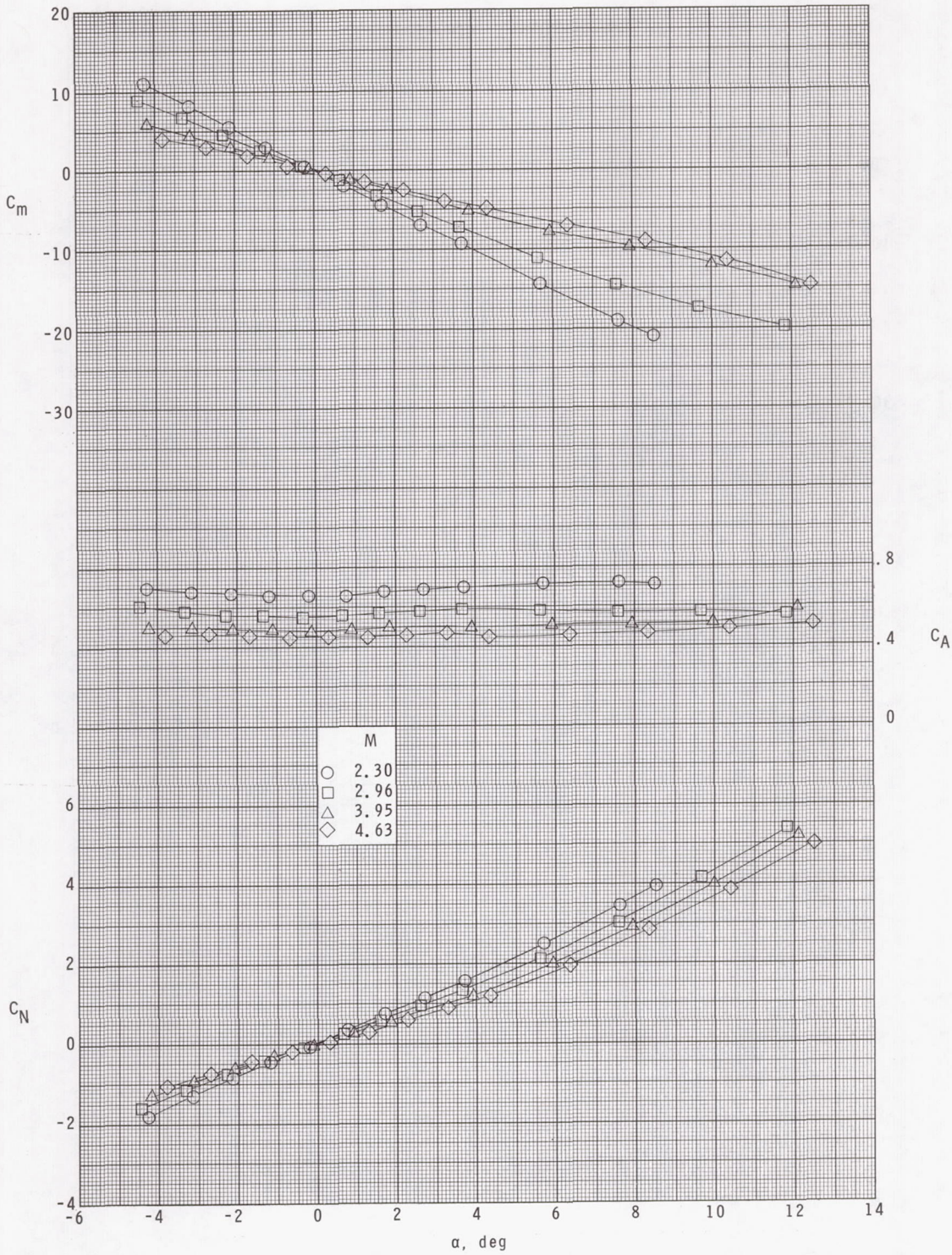

(a) $\Phi = 0^{\circ}$.

Figure 4.- Longitudinal aerodynamic characteristics of model with forward-positioned quadraloop antennas.

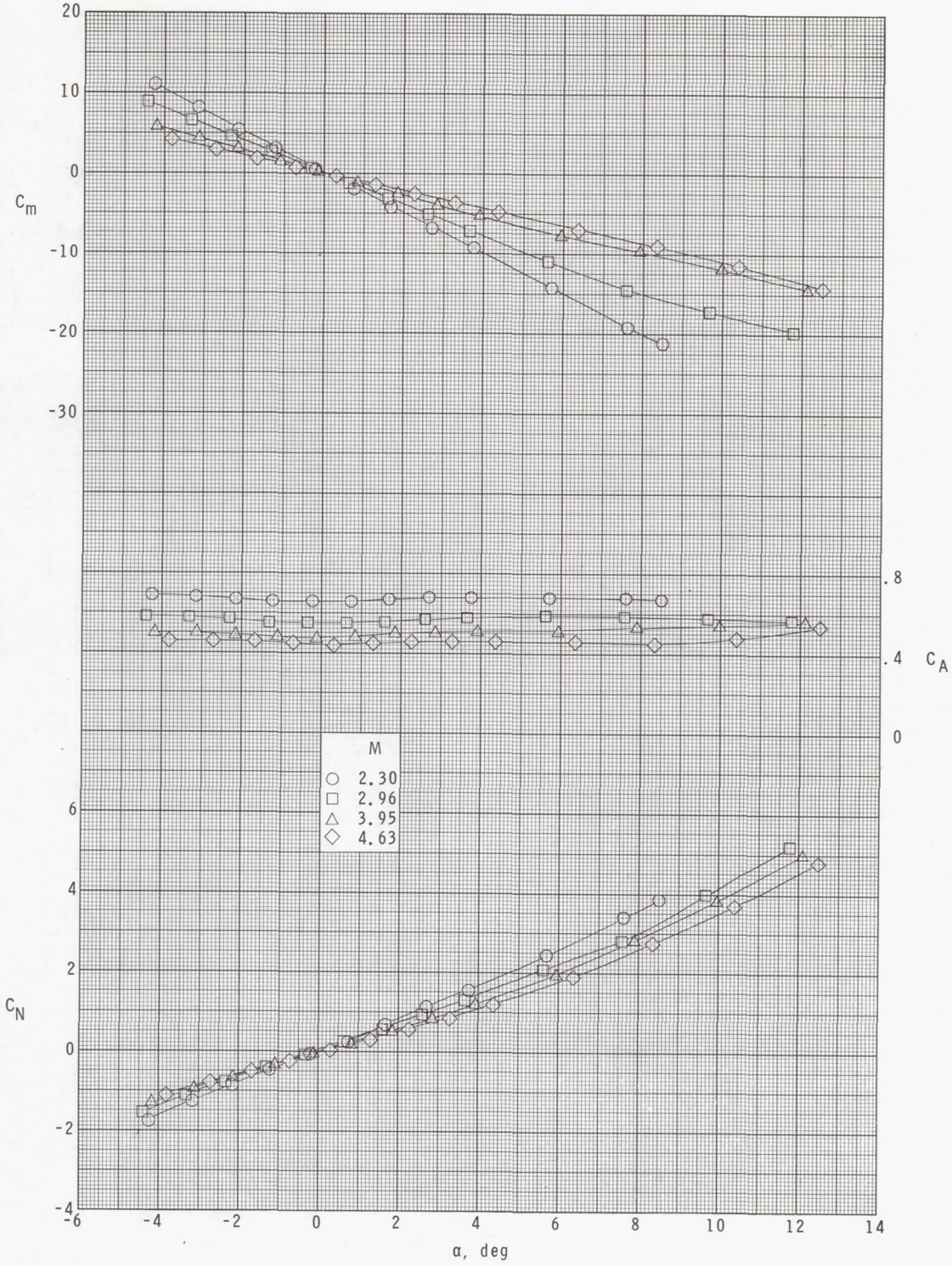

(b) $\Phi = 22.5^{\circ}$.

Figure 4.- Continued.

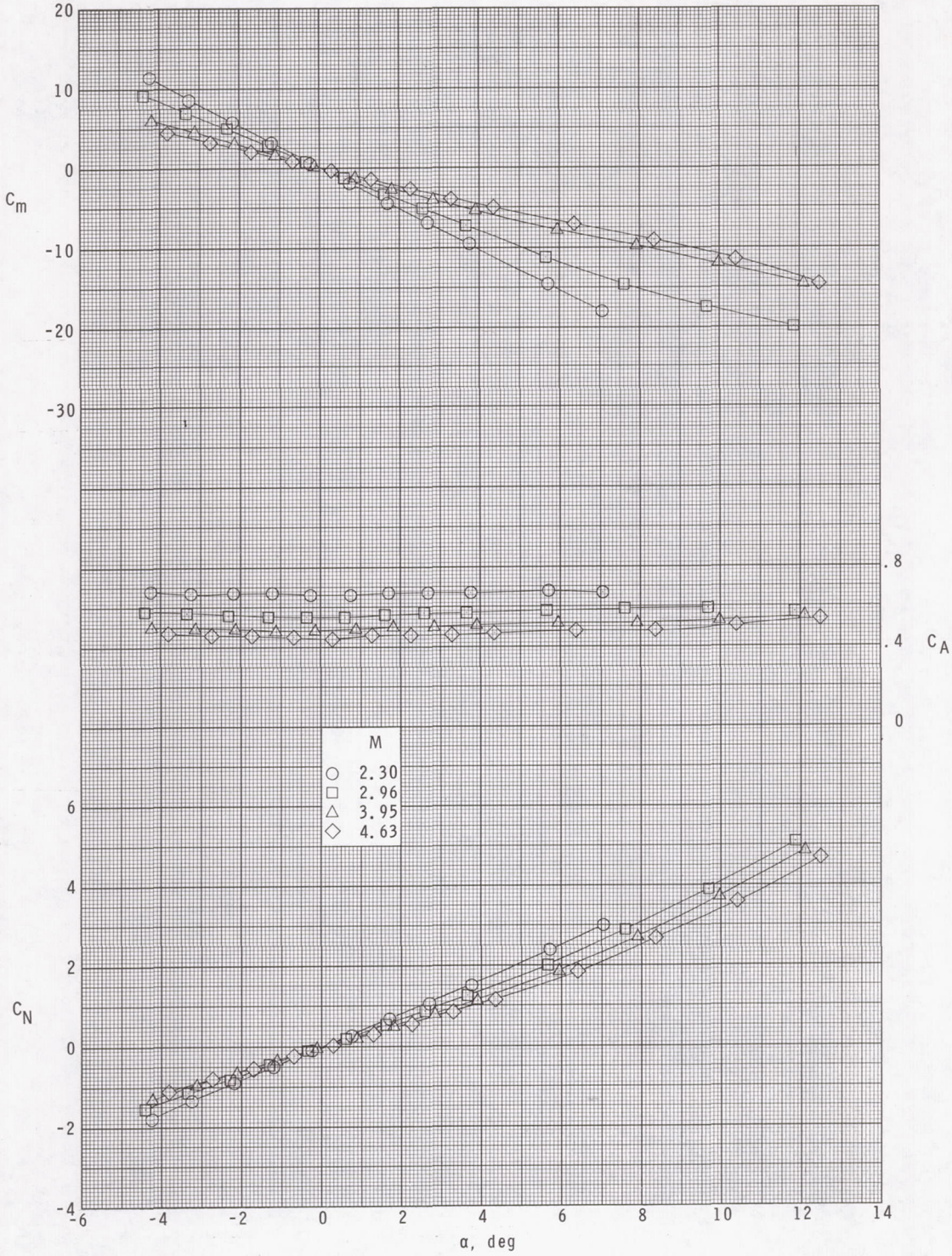

(c) $\Phi = 45^{\circ}$.

Figure 4.- Concluded.

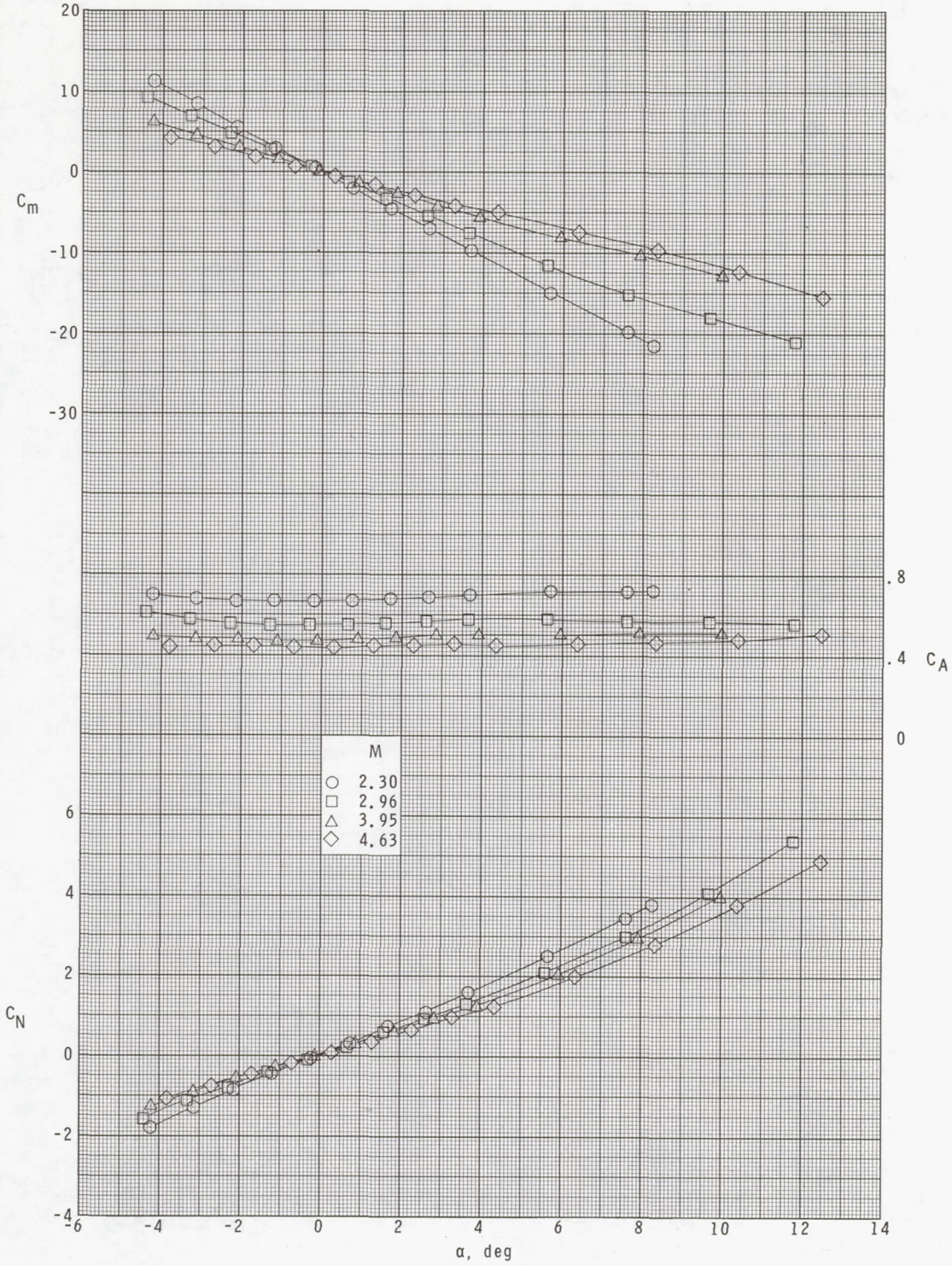

(a) $\Phi = 0^{0}$.

Figure 5.- Longitudinal aerodynamic characteristics of model with rearward-positioned quadraloop antennas.

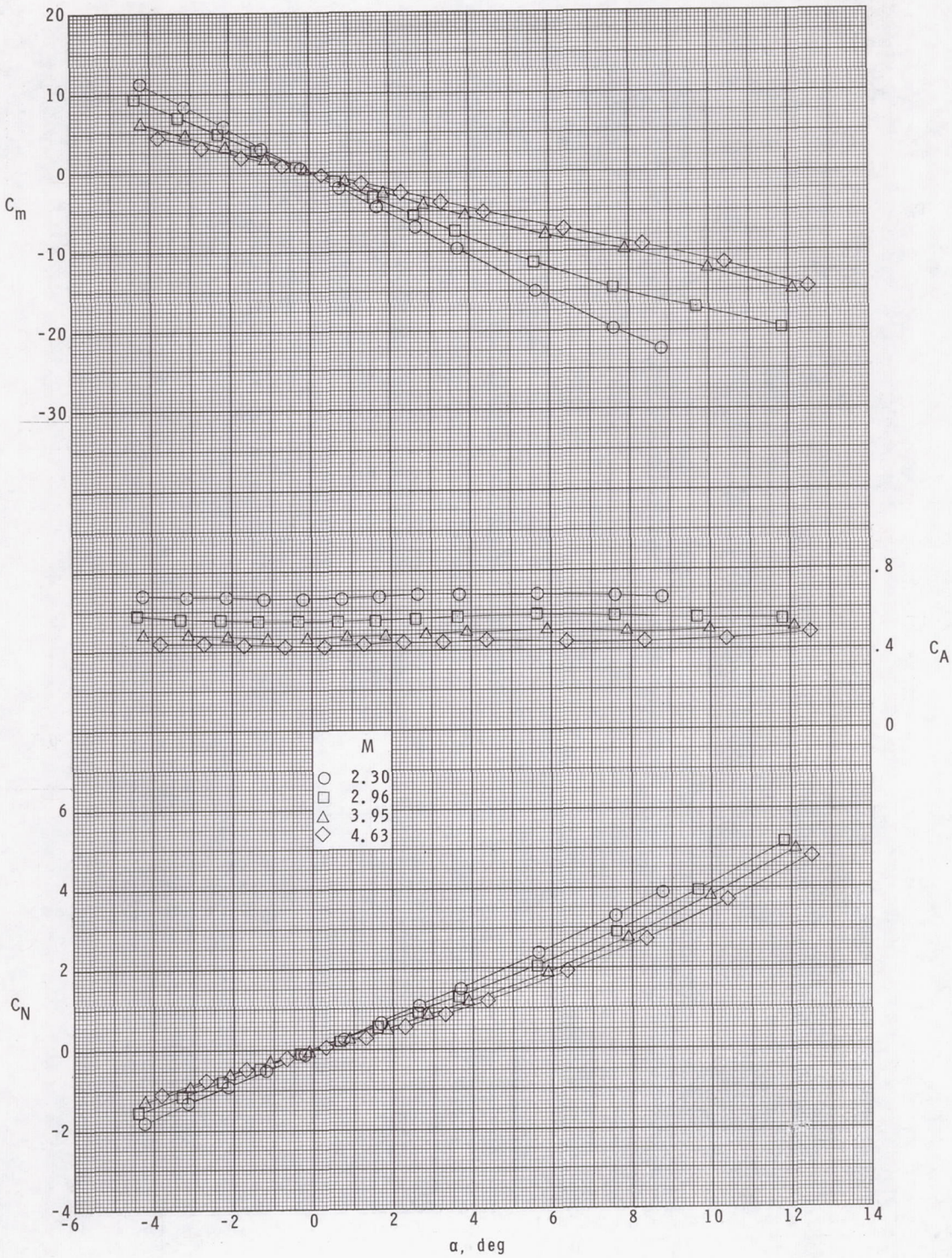

(b) $\Phi = 22.5^{\circ}$.

Figure 5.- Continued.

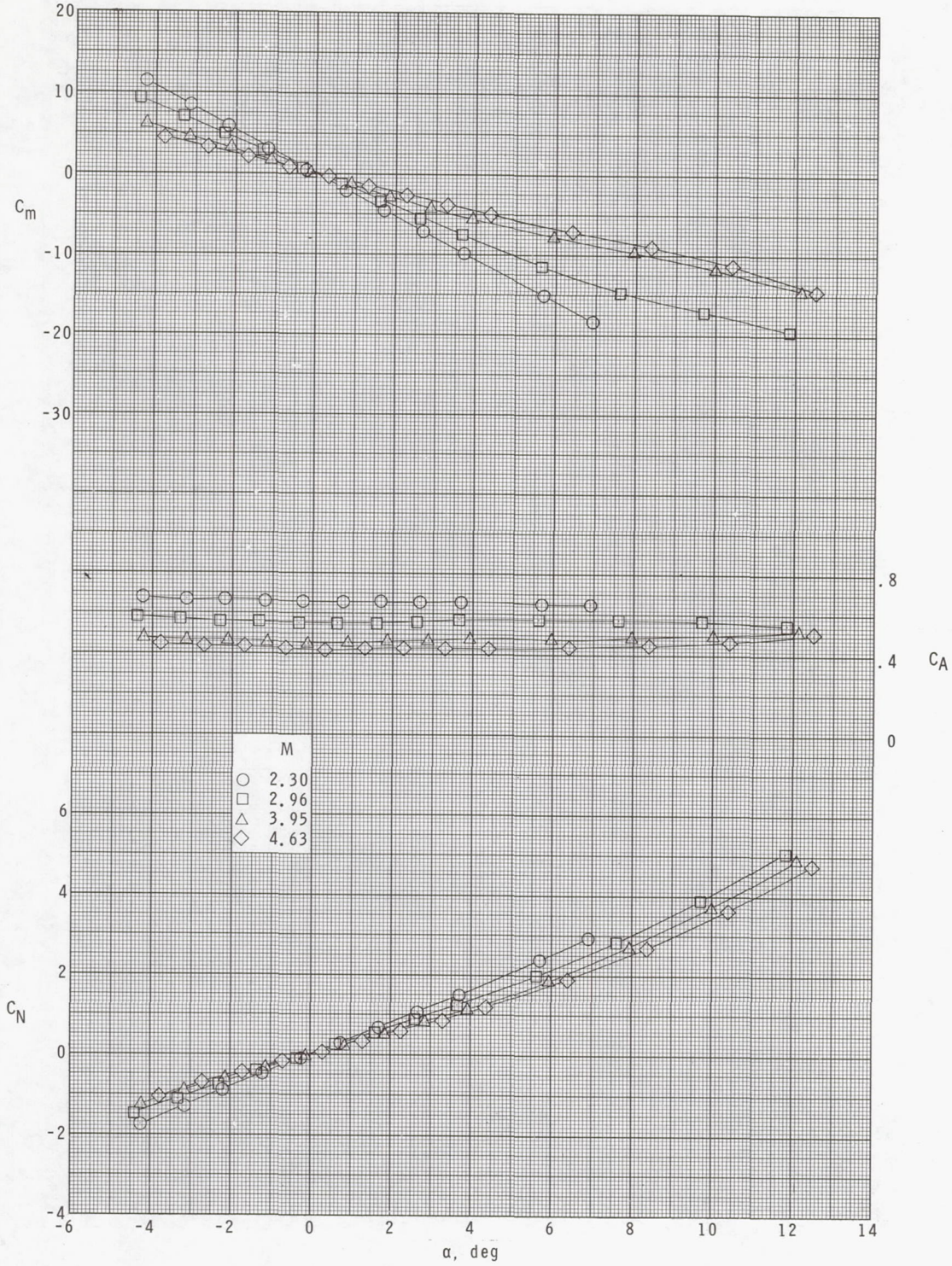

(c) $\Phi = 45^{\circ}$.

Figure 5.- Concluded.

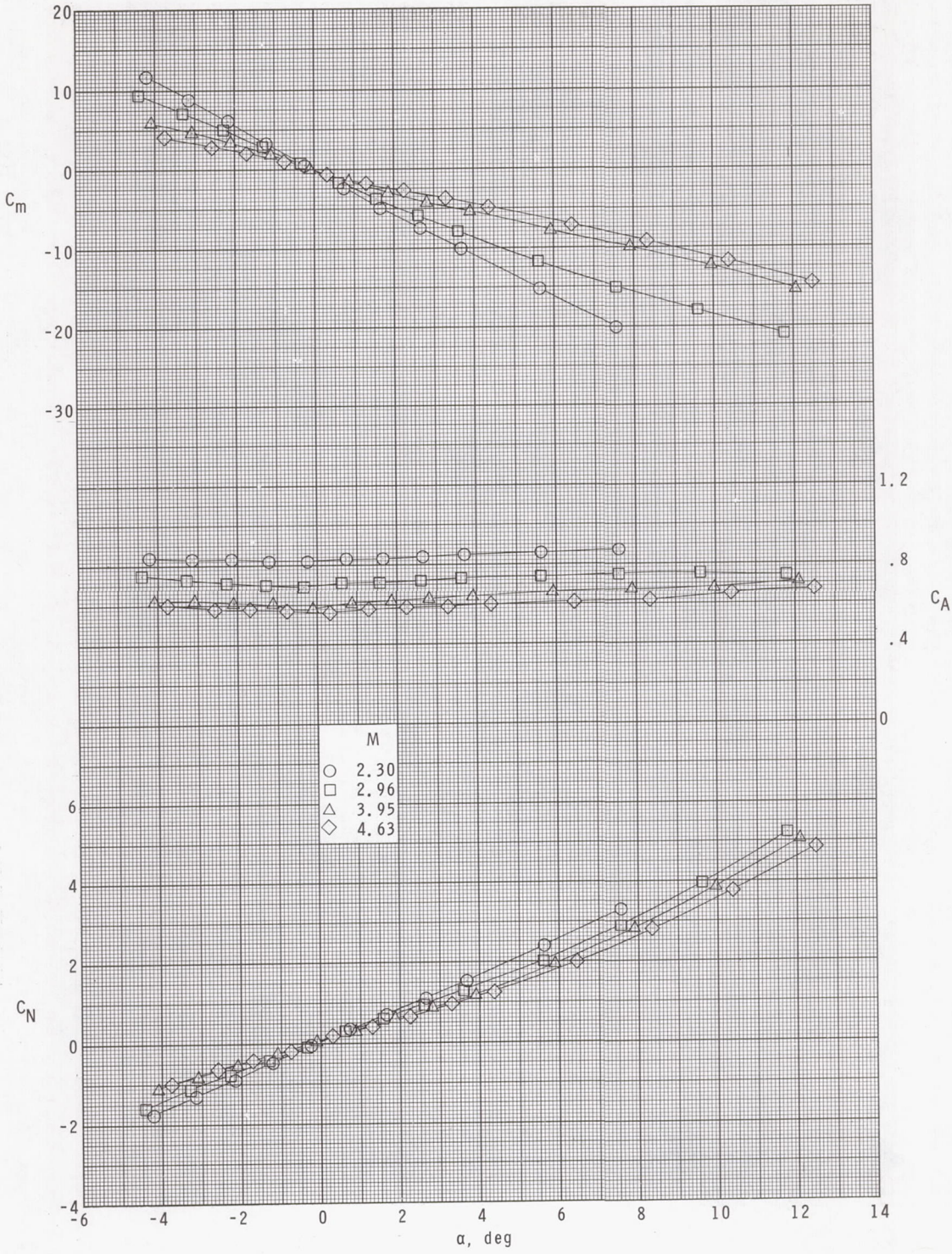

(a) $\Phi = 0^{\circ}$.

Figure 6.- Longitudinal aerodynamic characteristics of model with turnstile antennas.

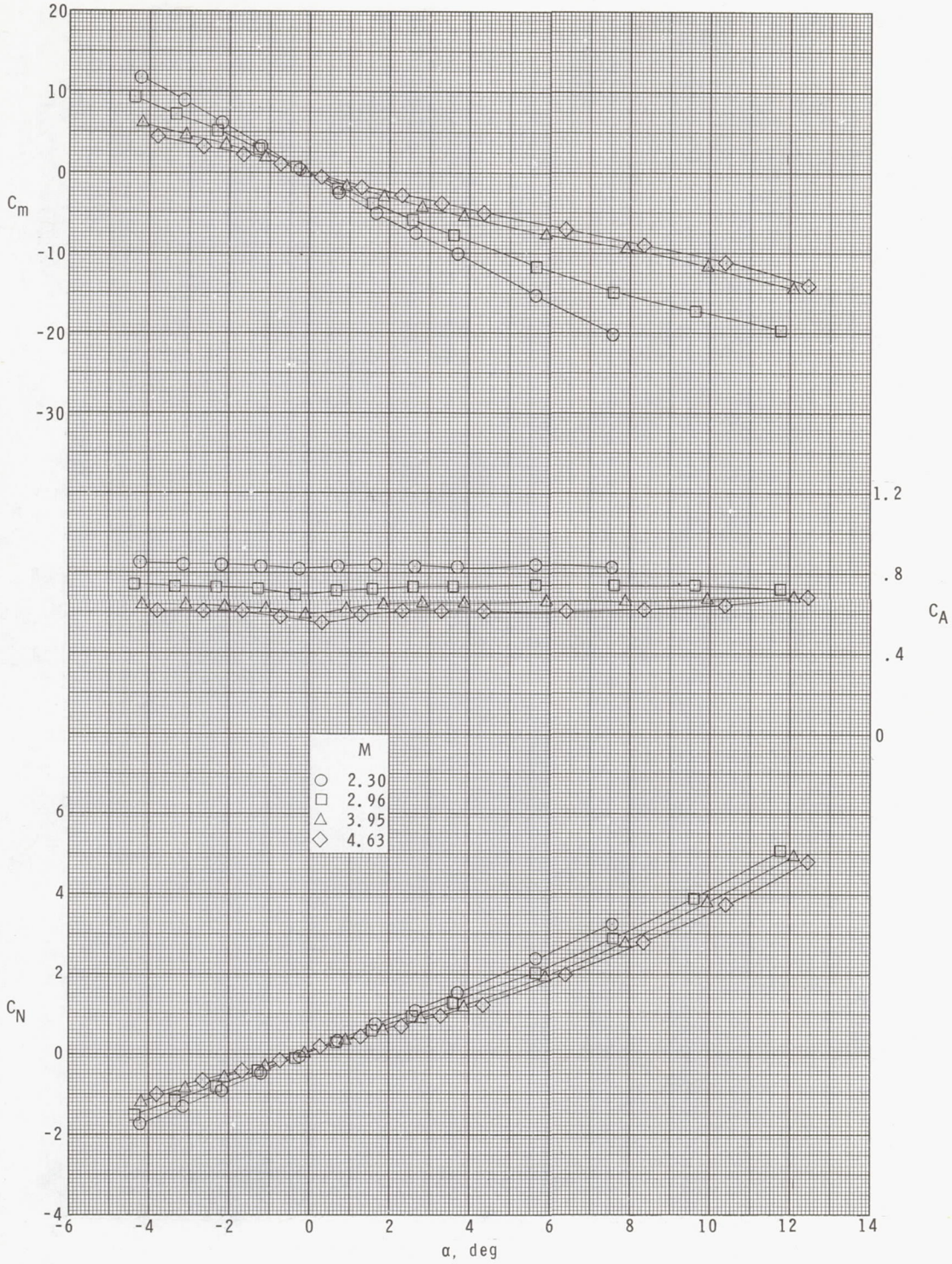

(b) $\Phi = 22.5^{\circ}$.

Figure 6.- Continued.

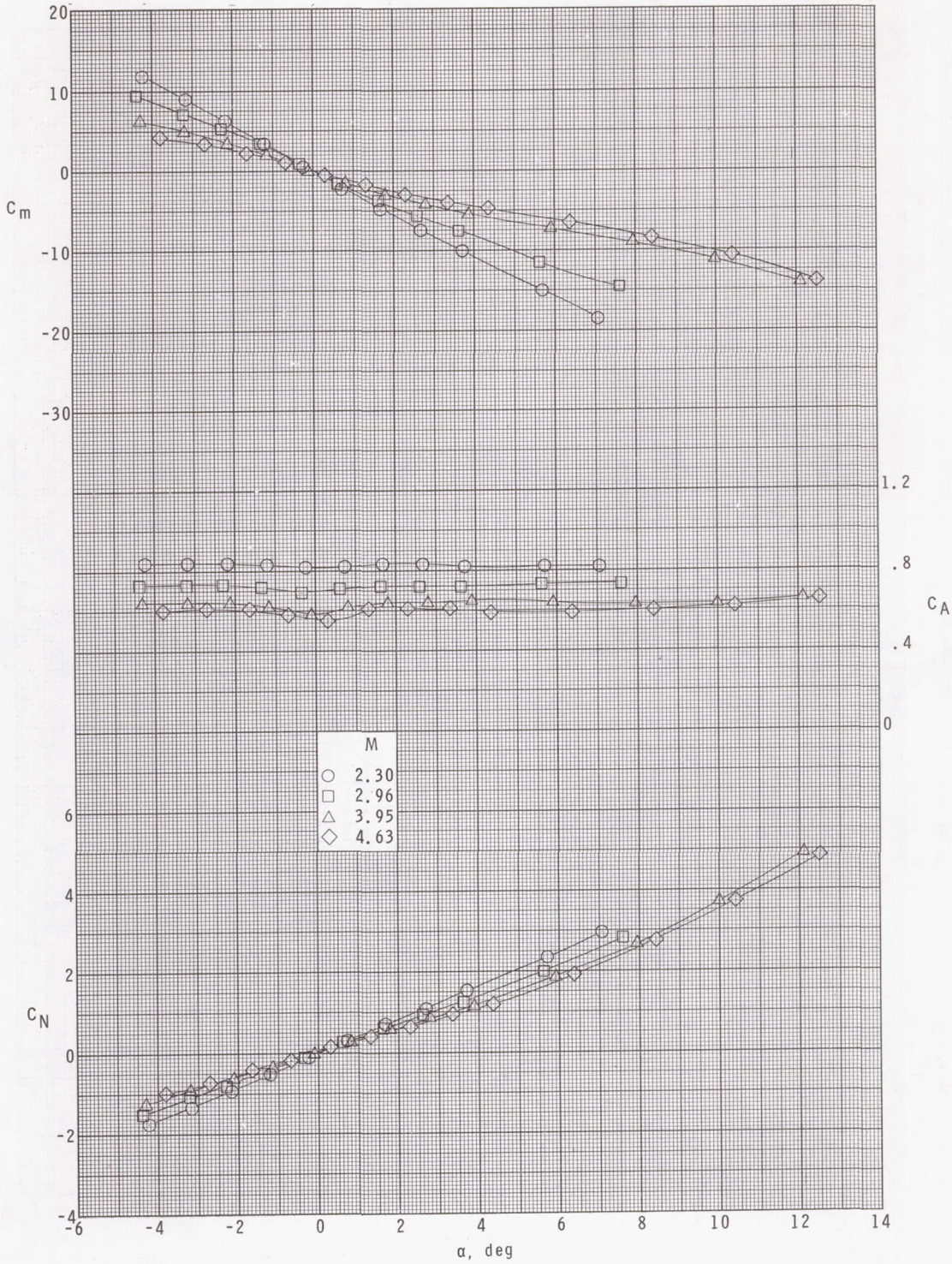

(c) $\Phi = 45^{\circ}$.

Figure 6.- Concluded.

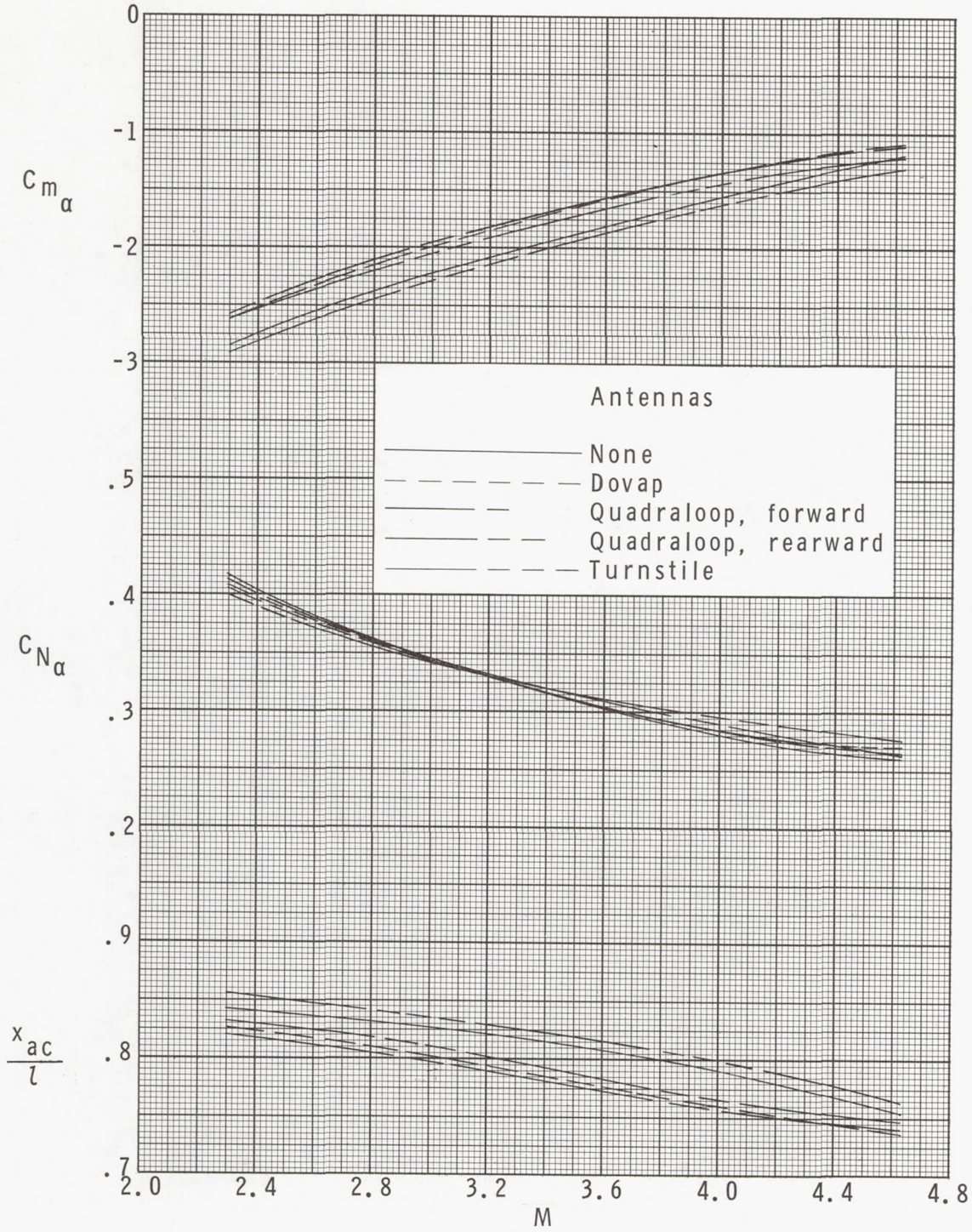

(a) $\Phi = 0^{\circ}$.

Figure 7.- Summary of longitudinal stability characteristics of model with the various antenna arrangements. $\alpha \approx 0^{\circ}$.

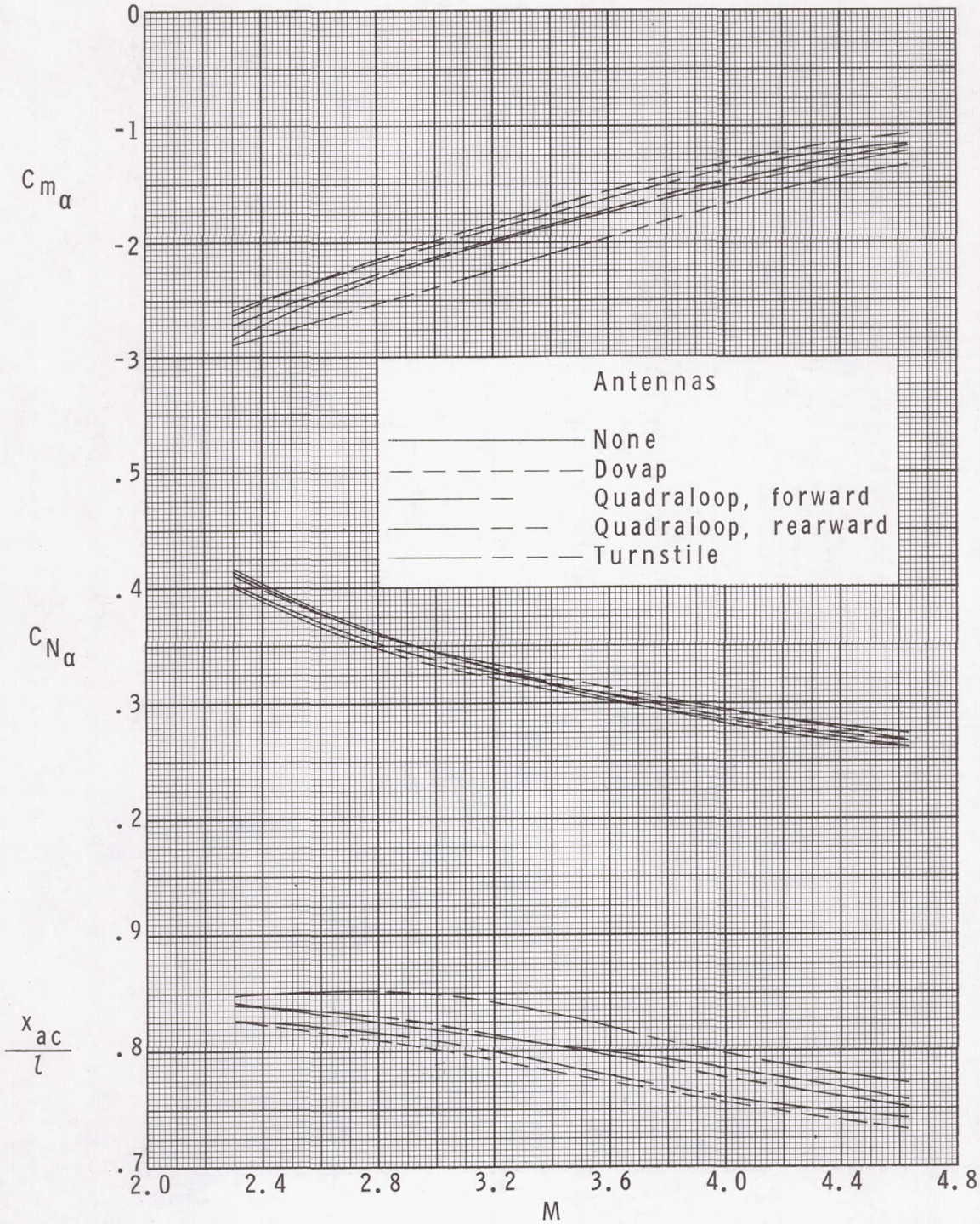

(b) $\Phi = 45^{\circ}$.

Figure 7.- Concluded.

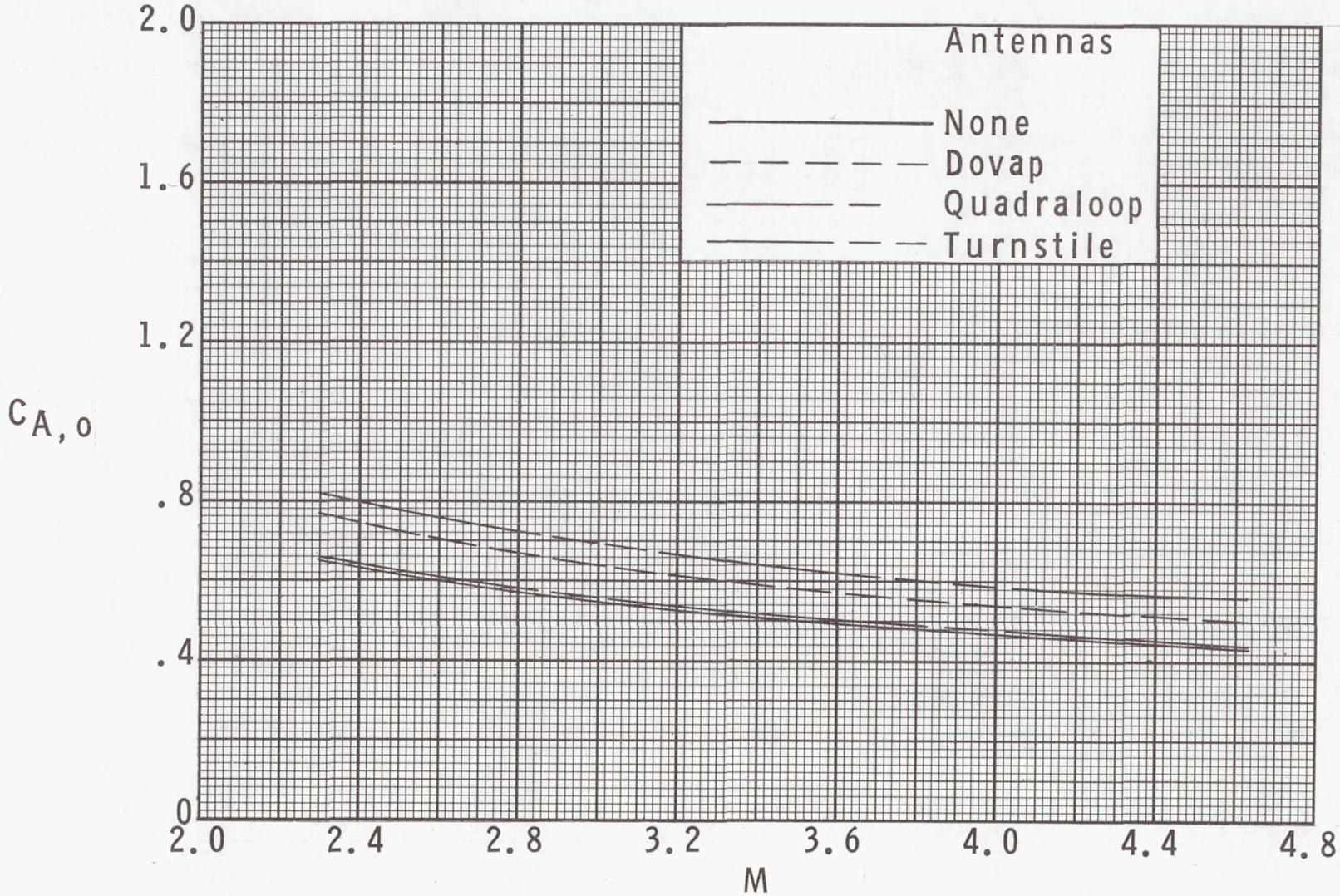

Figure 8.- Axial-force coefficient at zero angle of attack for the various antenna arrangements.

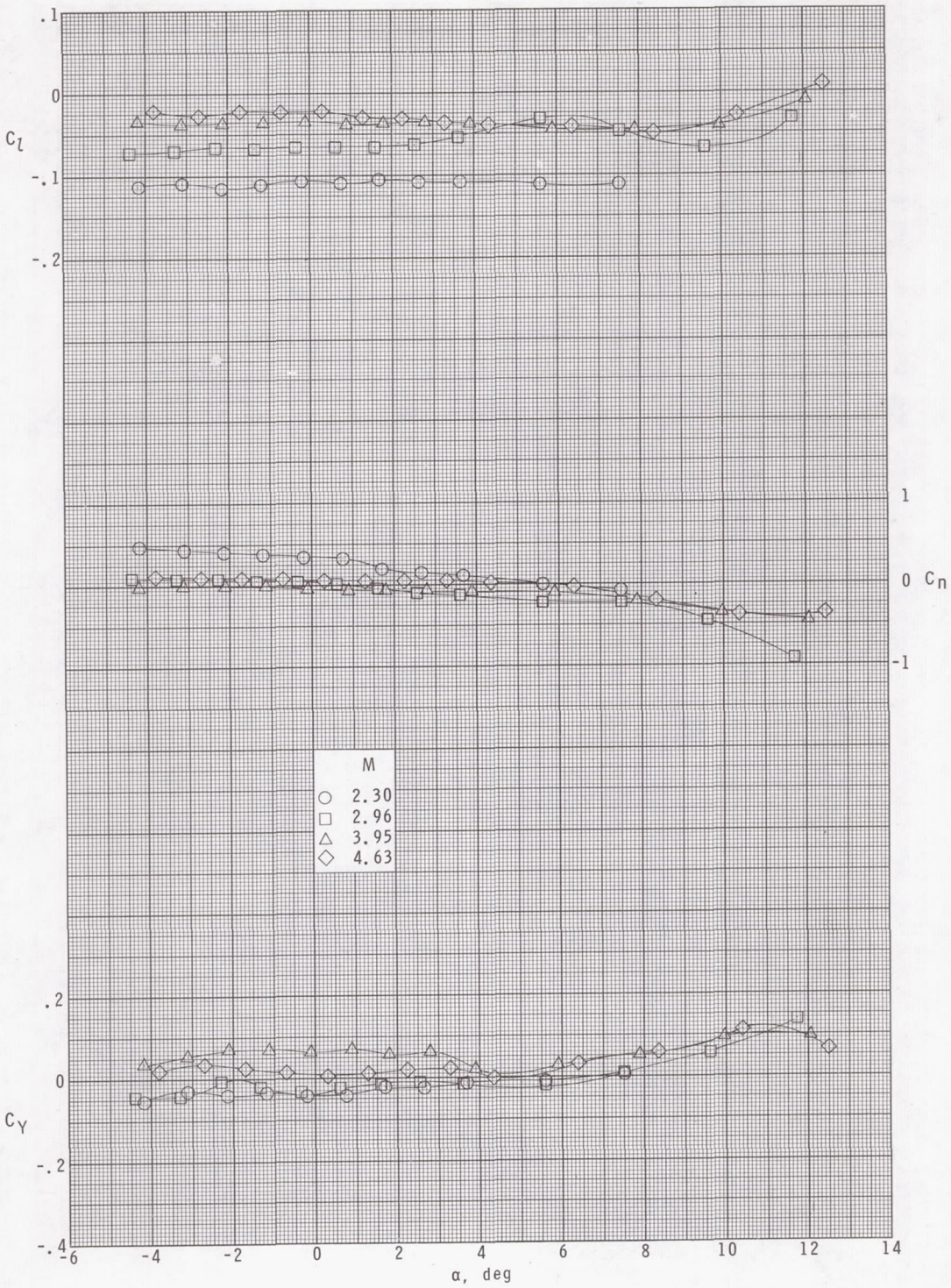

(a) $\Phi = 0^{\circ}$.

Figure 9.- Lateral aerodynamic characteristics of clean configuration (no antennas).

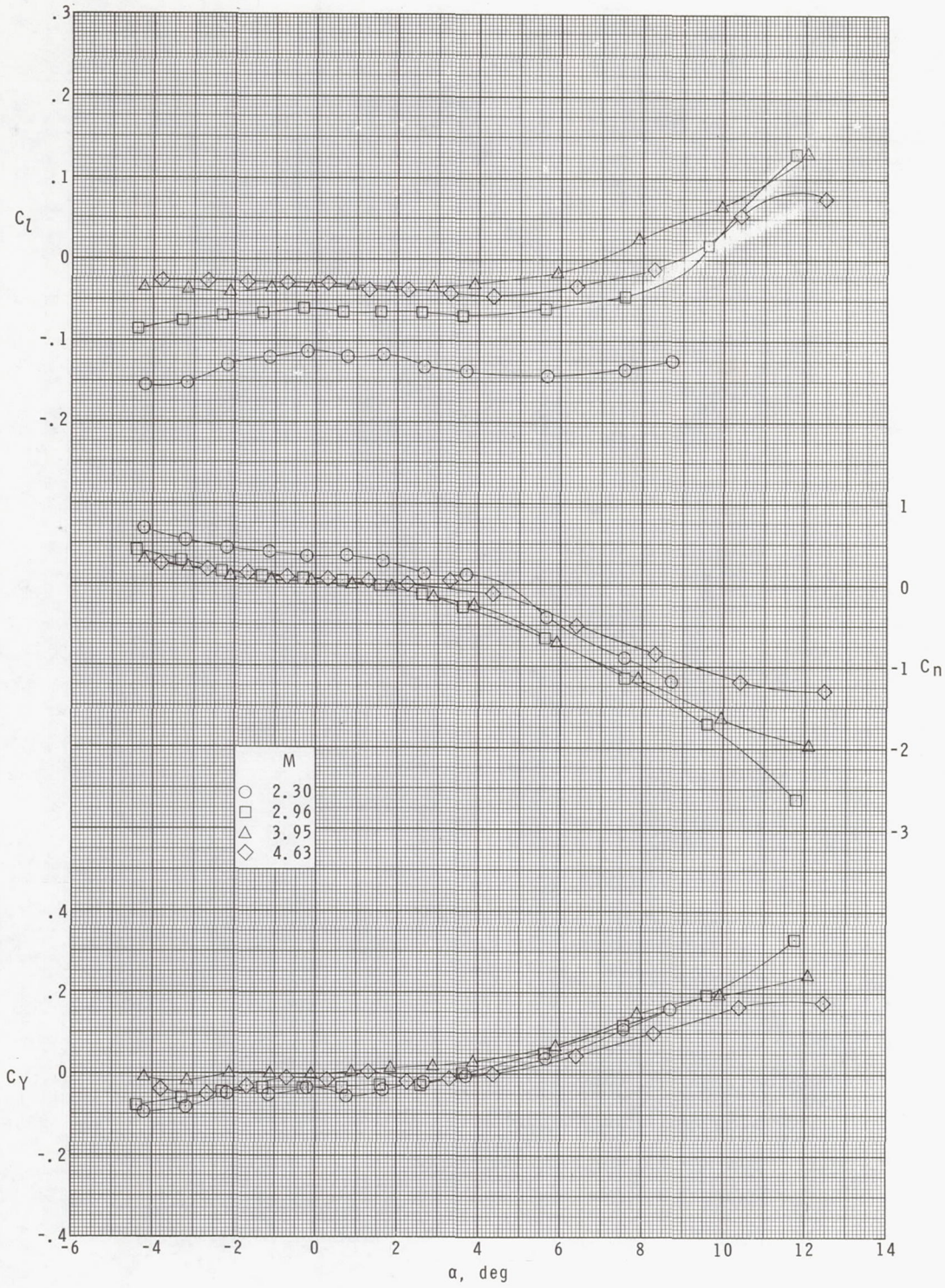

(b) $\Phi = 22.5^{\circ}$.

Figure 9.- Continued.

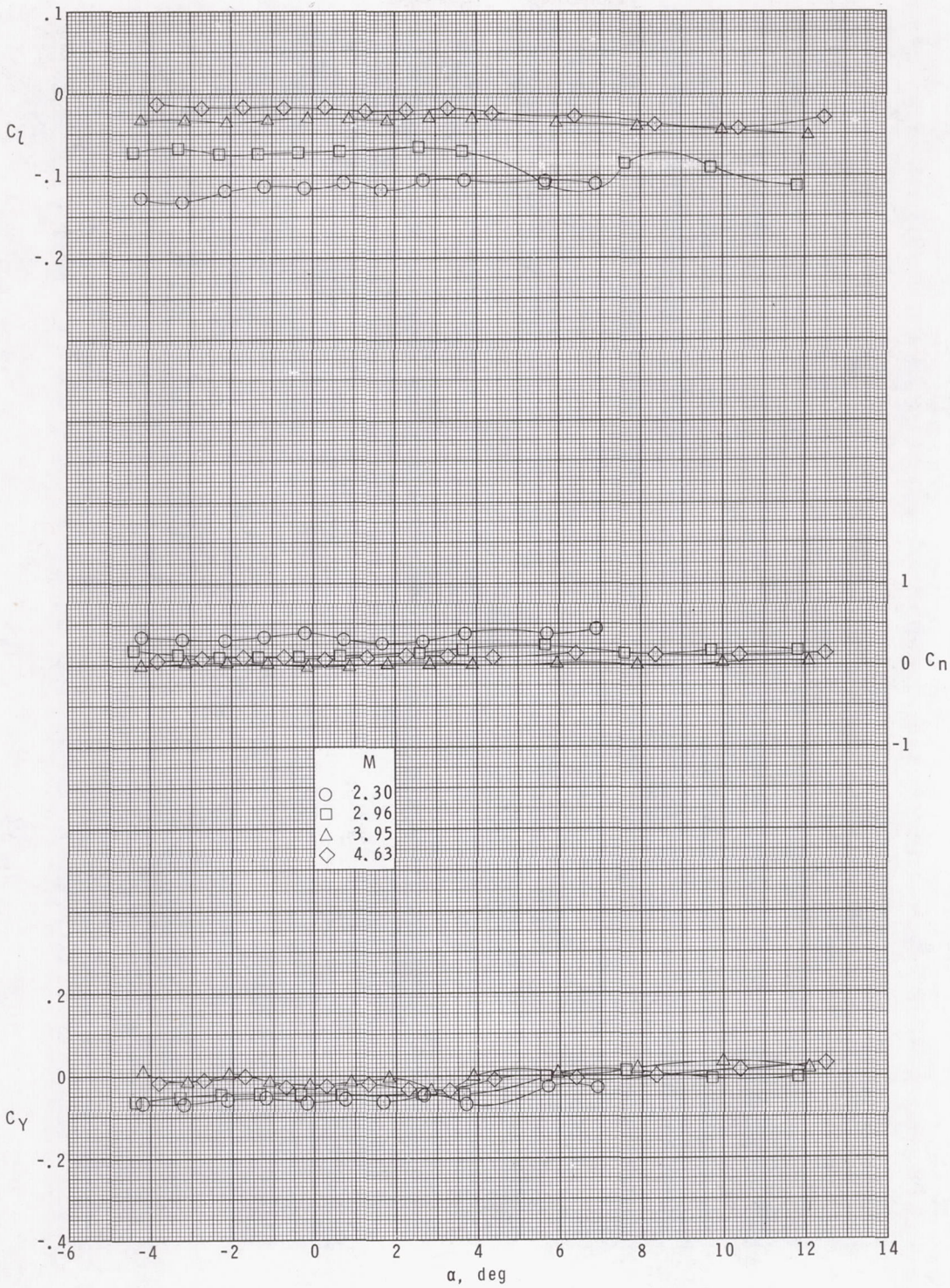

(c) $\Phi = 45^{\circ}$.

Figure 9.- Concluded.

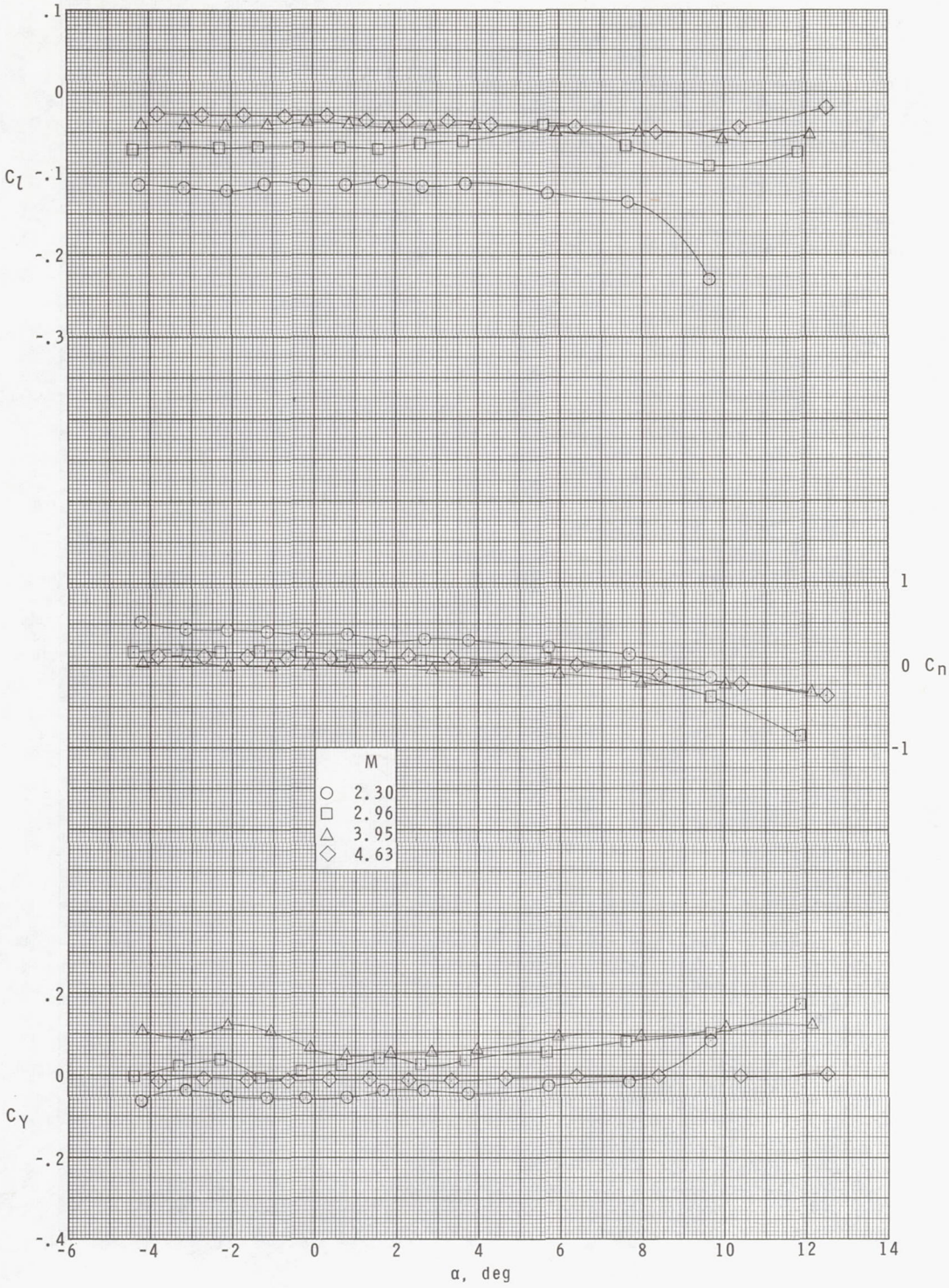

(a) $\Phi = 0^{\circ}$.

Figure 10.- Lateral aerodynamic characteristics of model with Dovap antennas.

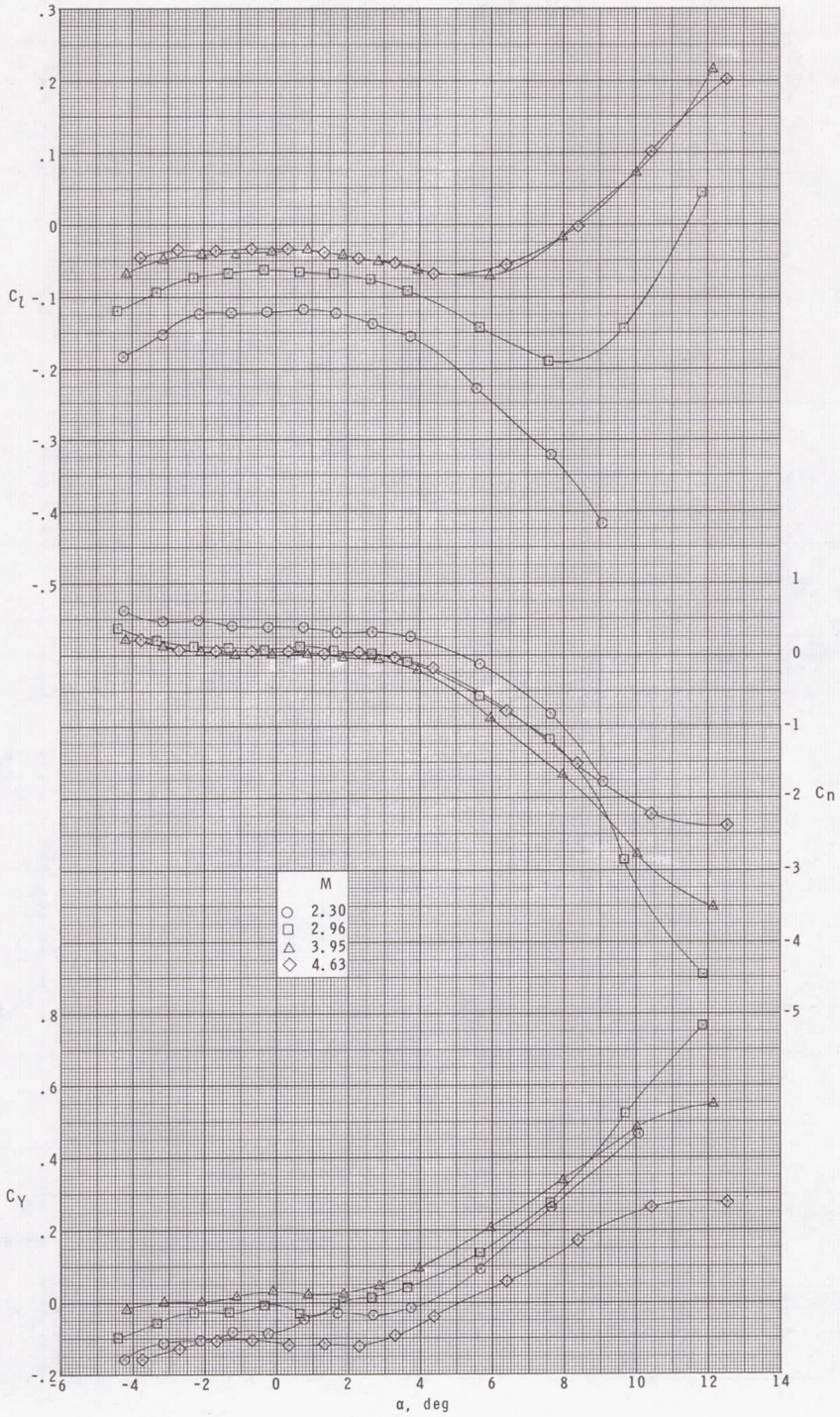

(b) $\Phi = 22.5^{\circ}$.

Figure 10.- Continued.

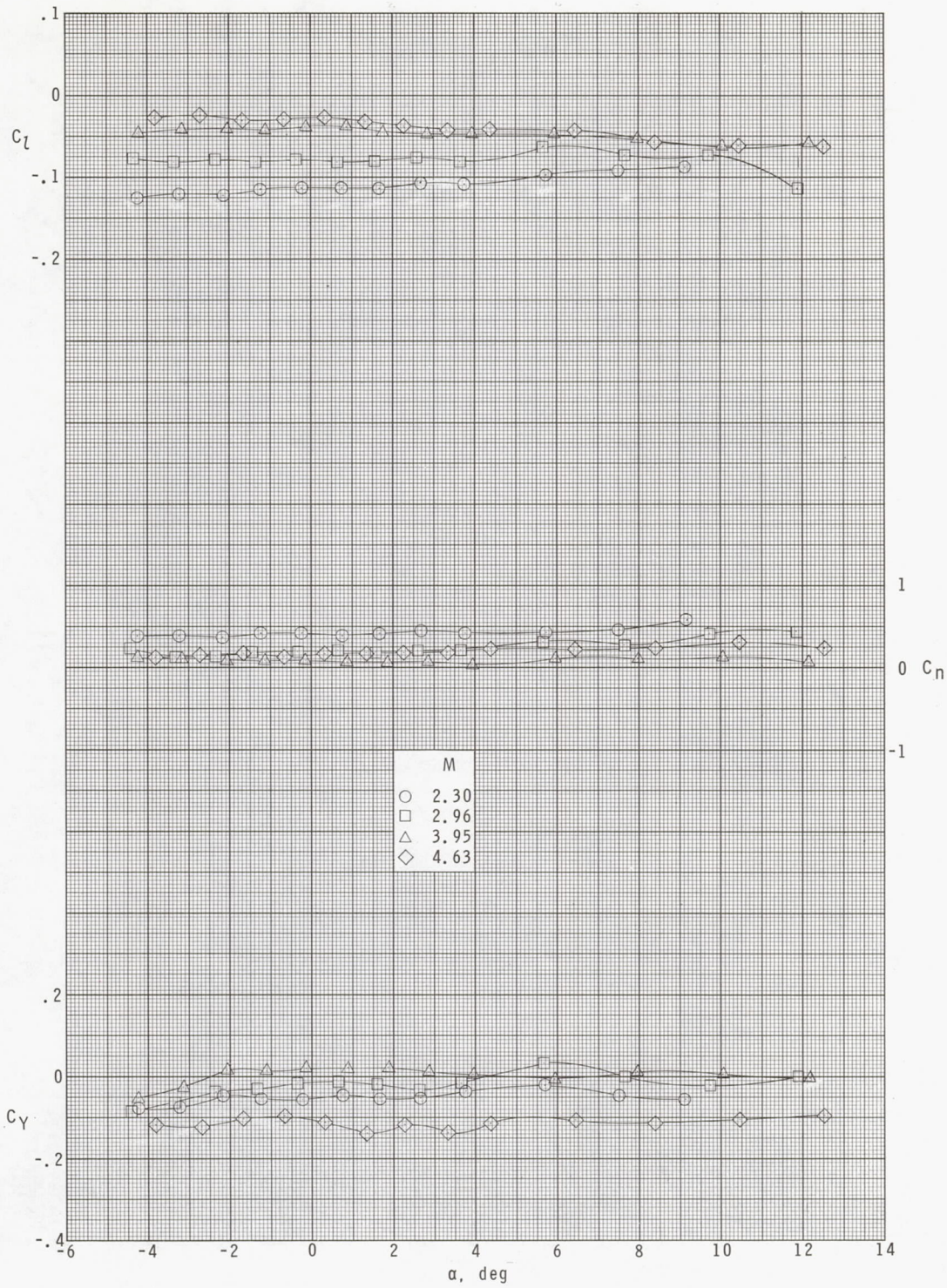

(c) $\Phi = 45^{\circ}$.

Figure 10.- Concluded.

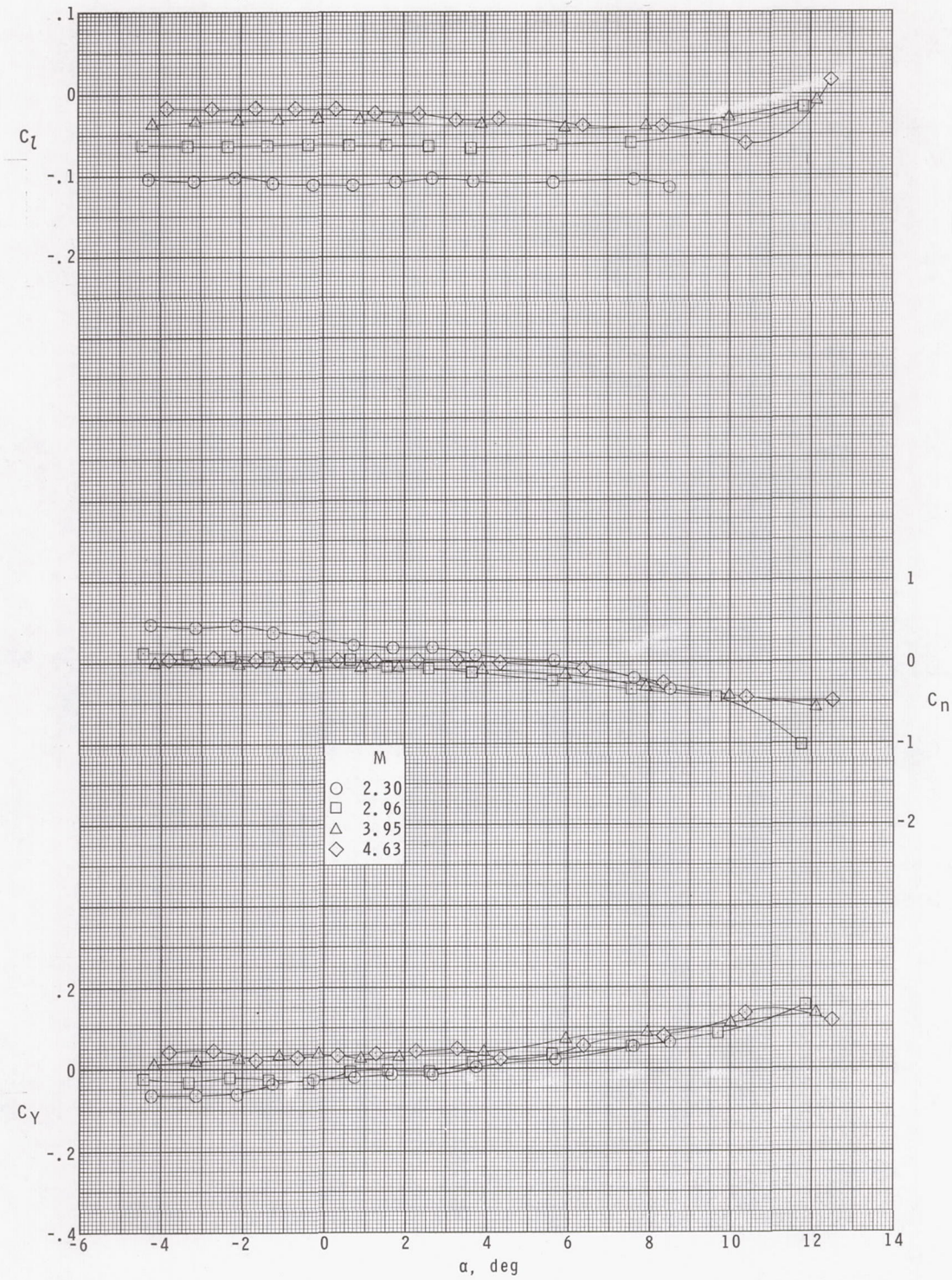

(a) $\Phi = 0^{\circ}$.

Figure 11.- Lateral aerodynamic characteristics of model with forward-positioned quadraloop antennas.

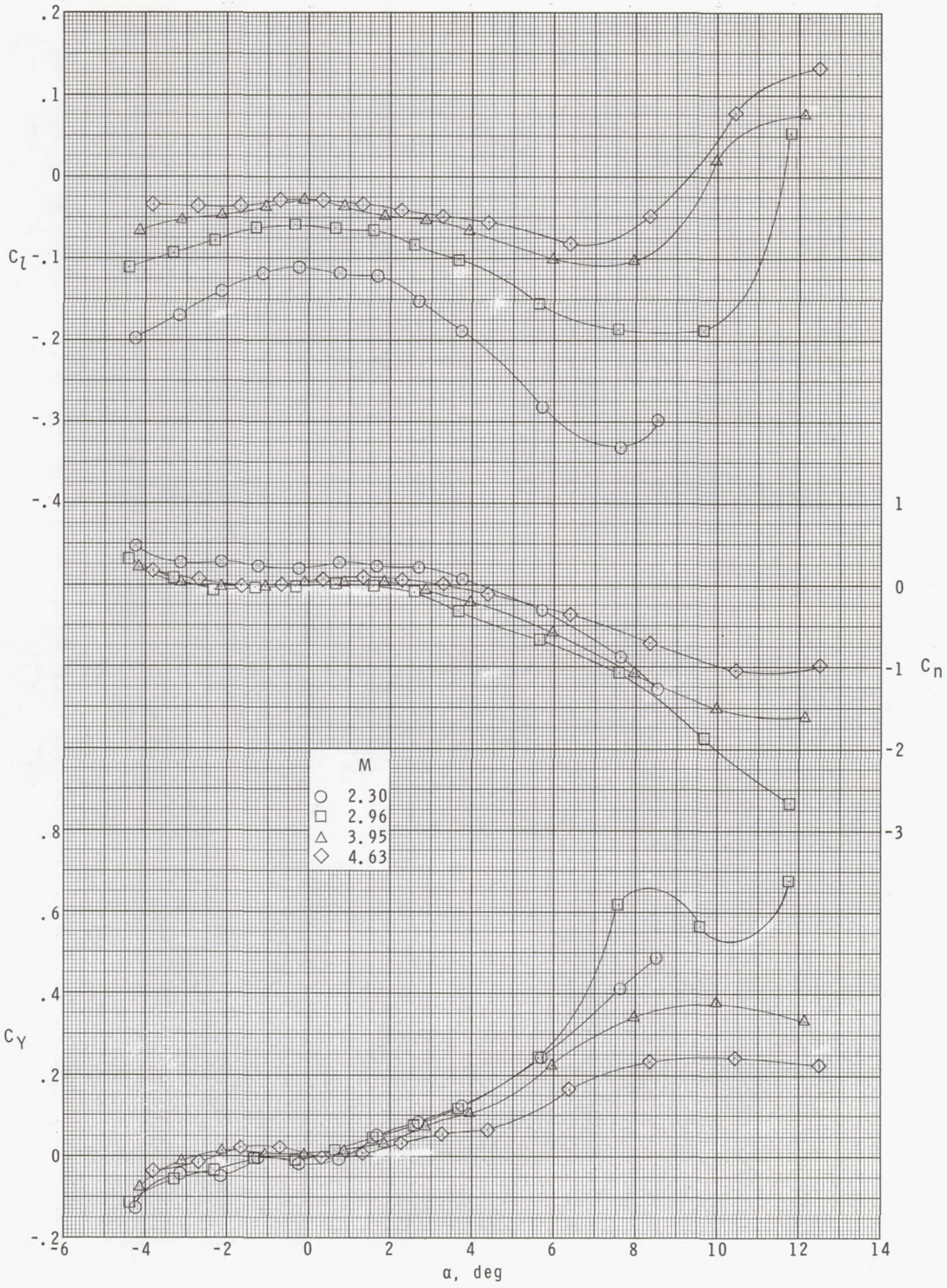

(b) $\Phi = 22.5^{\circ}$.

Figure 11.- Continued.

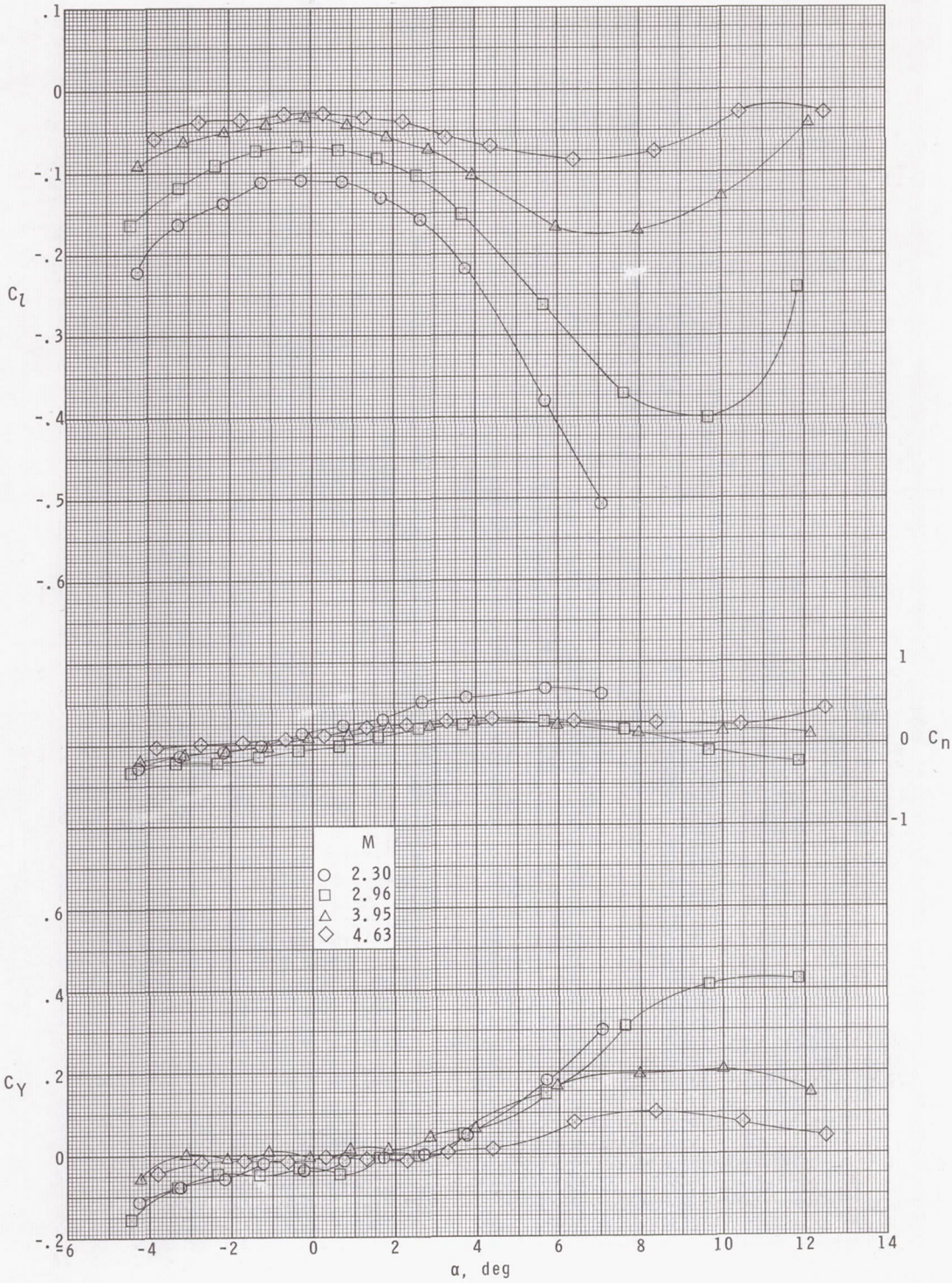

(c) $\Phi = 45^{\circ}$.

Figure 11.- Concluded.

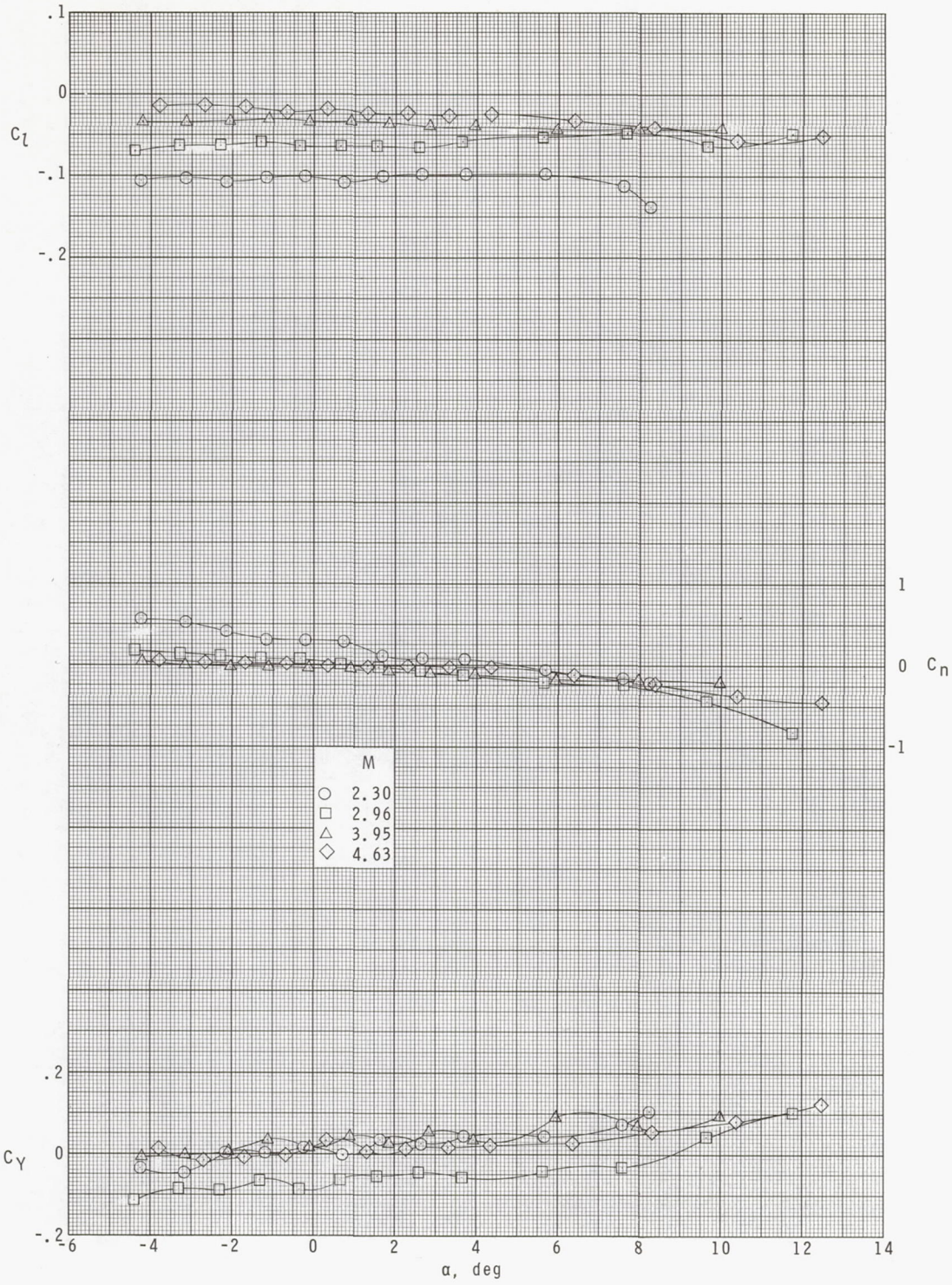

(a) $\Phi = 0^{\circ}$.

Figure 12.- Lateral aerodynamic characteristics of model with rearward-positioned quadraloop antennas.

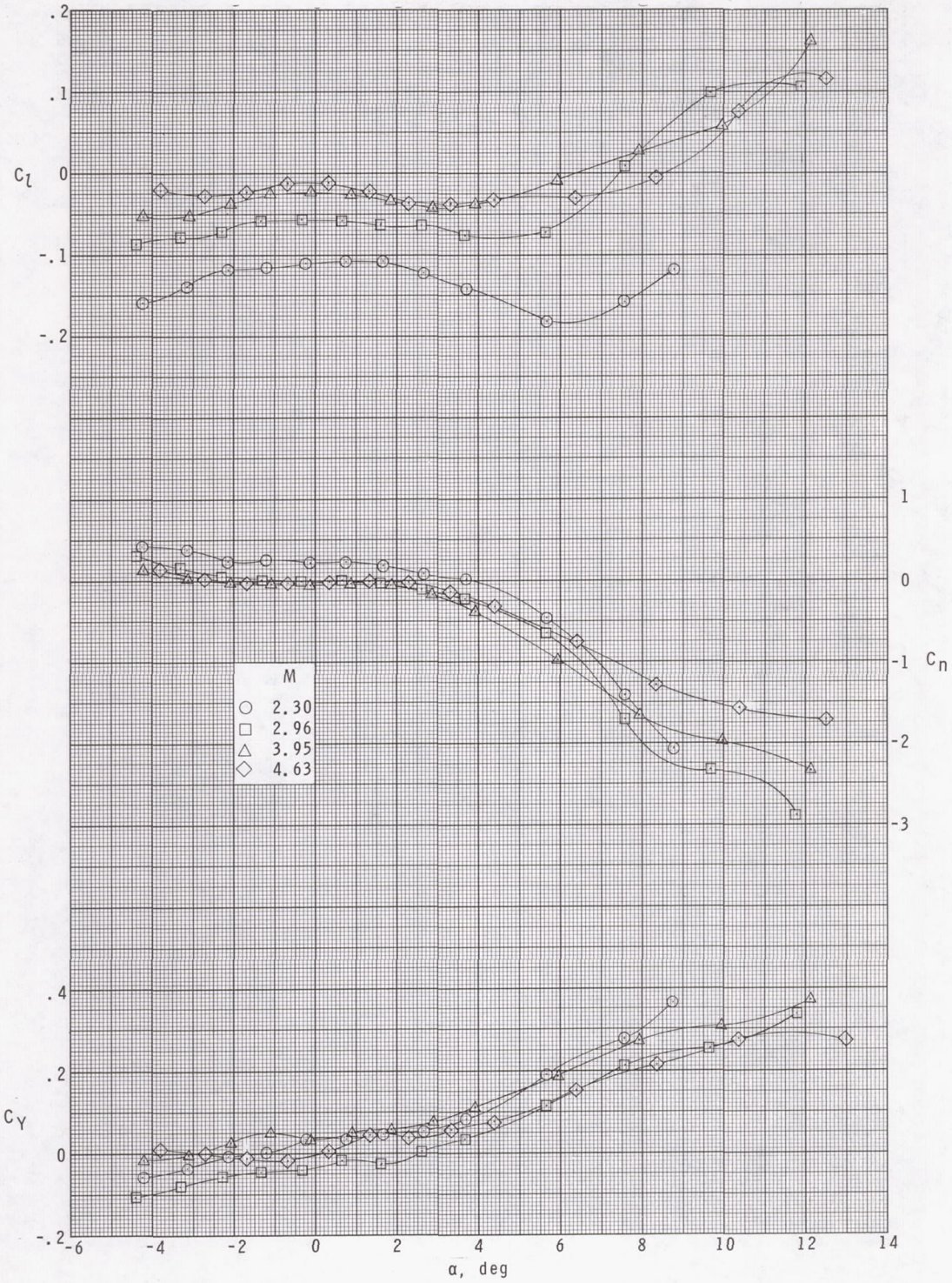

(b) $\Phi = 22.5^{\circ}$.

Figure 12.- Continued.

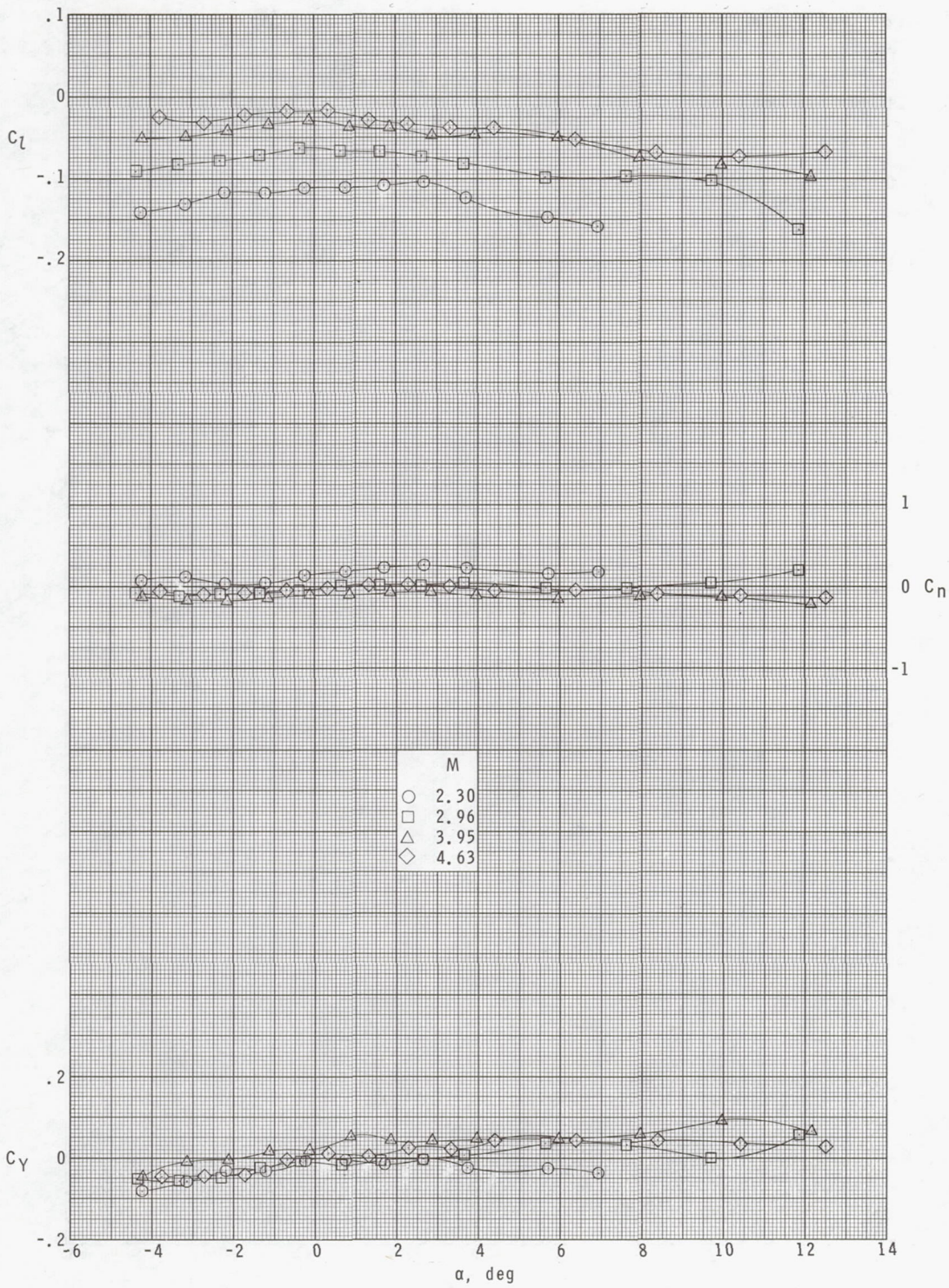

(c) $\Phi = 45^{\circ}$.

Figure 12.- Concluded.

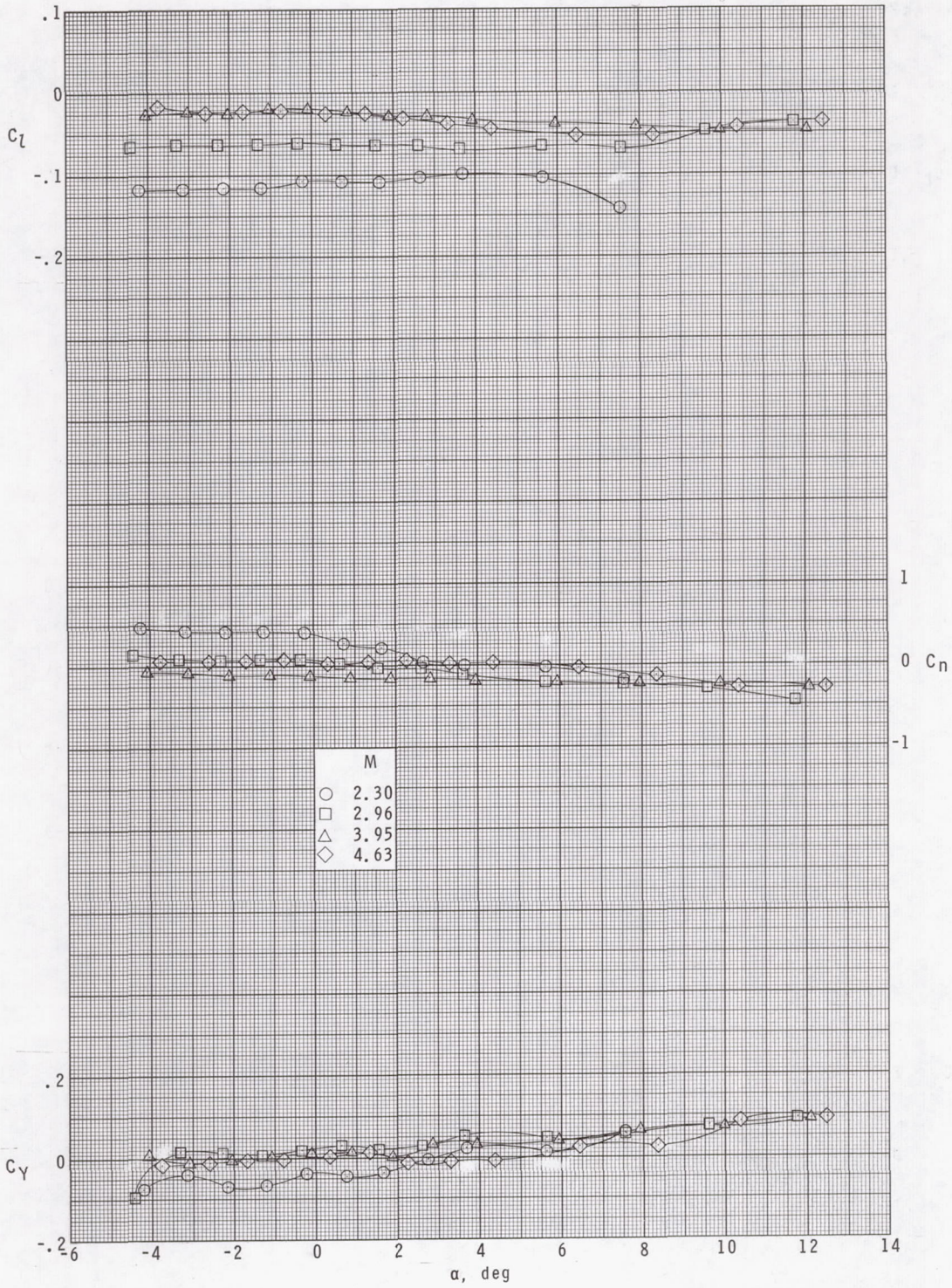

(a) $\Phi = 0^{\circ}$.

Figure 13.- Lateral aerodynamic characteristics of model with turnstile antennas.

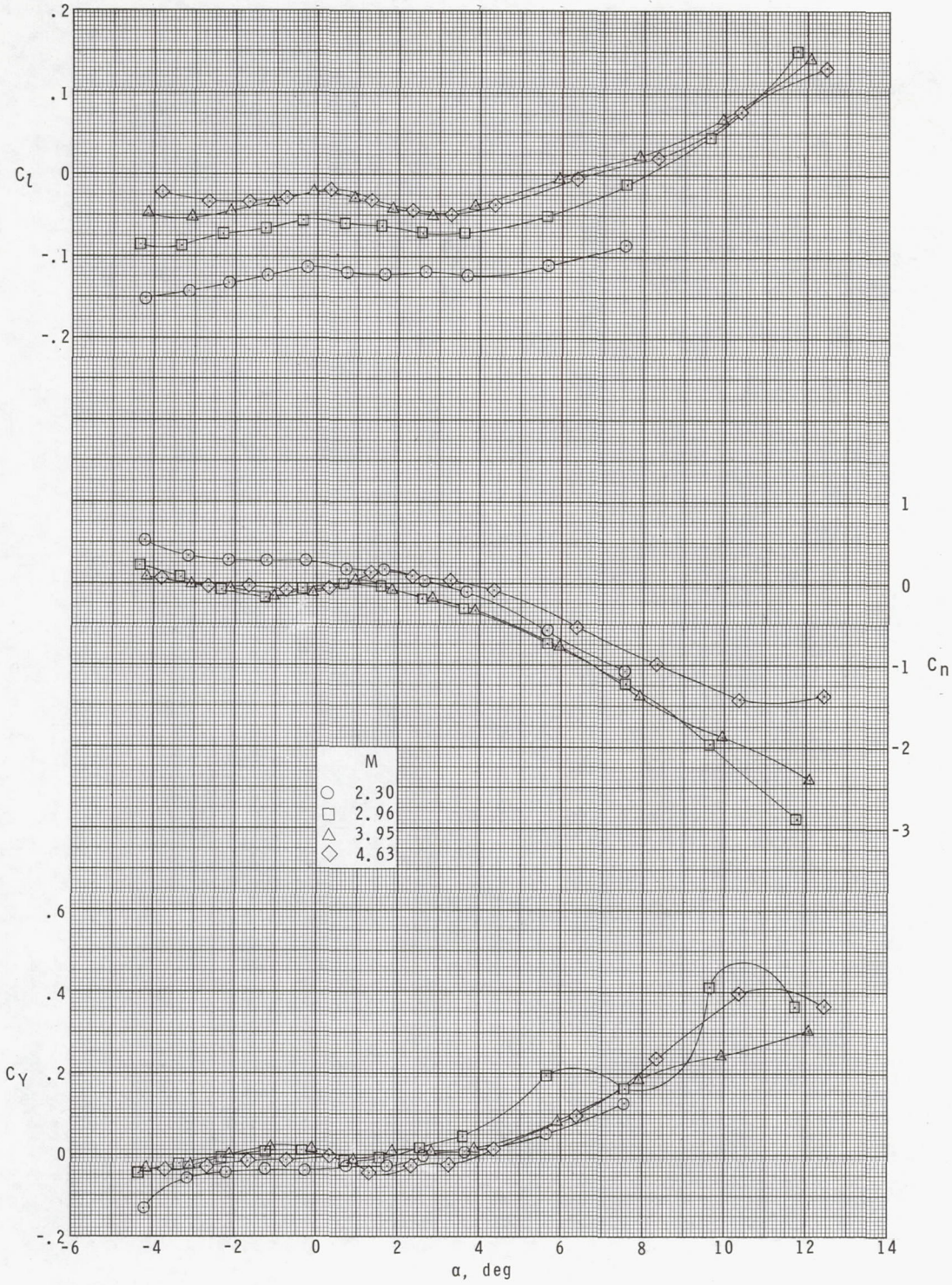

(b) $\Phi = 22.5^{\circ}$.

Figure 13.- Continued.

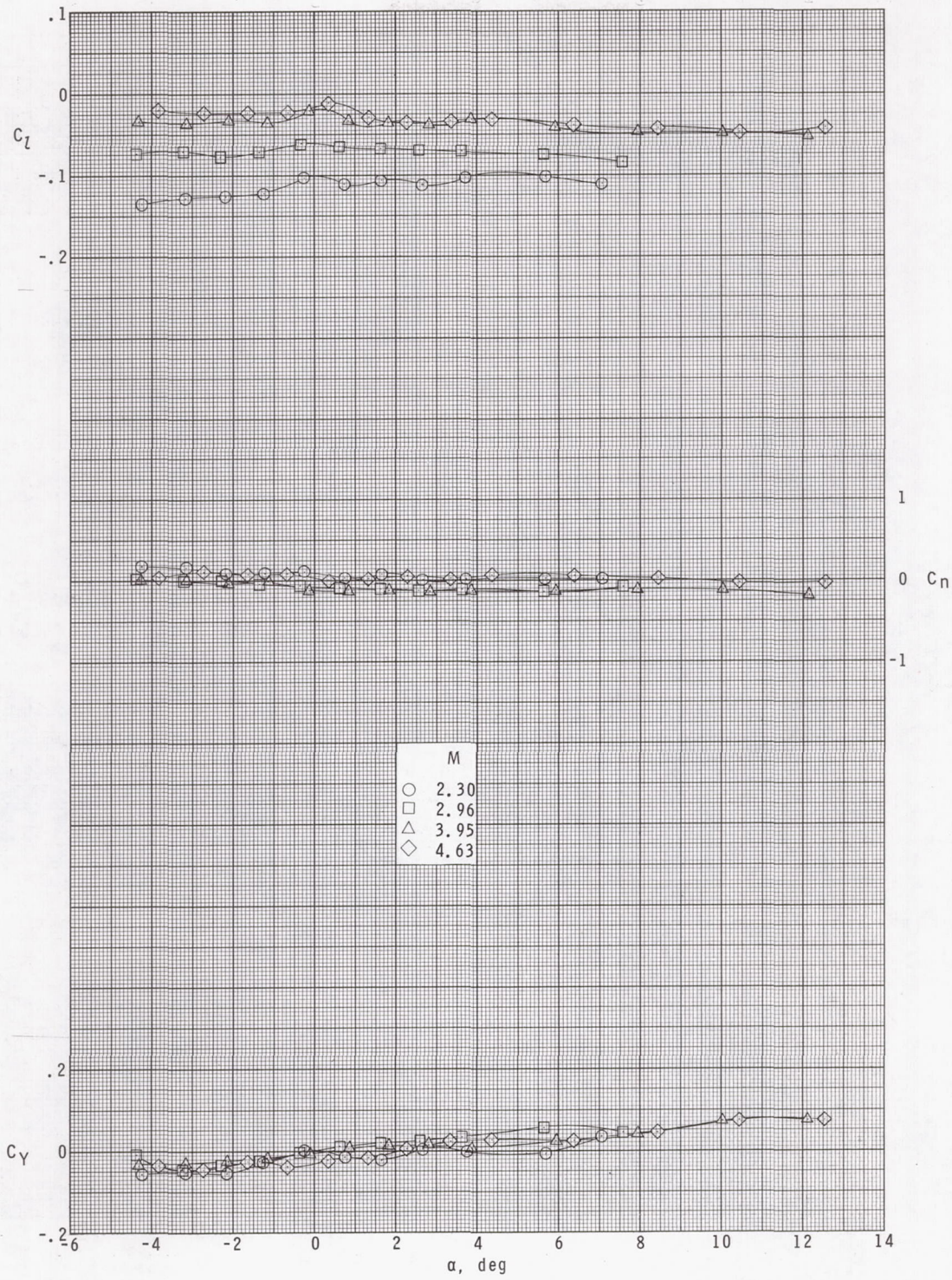

(c) $\Phi = 45^{\circ}$.

Figure 13.- Concluded.

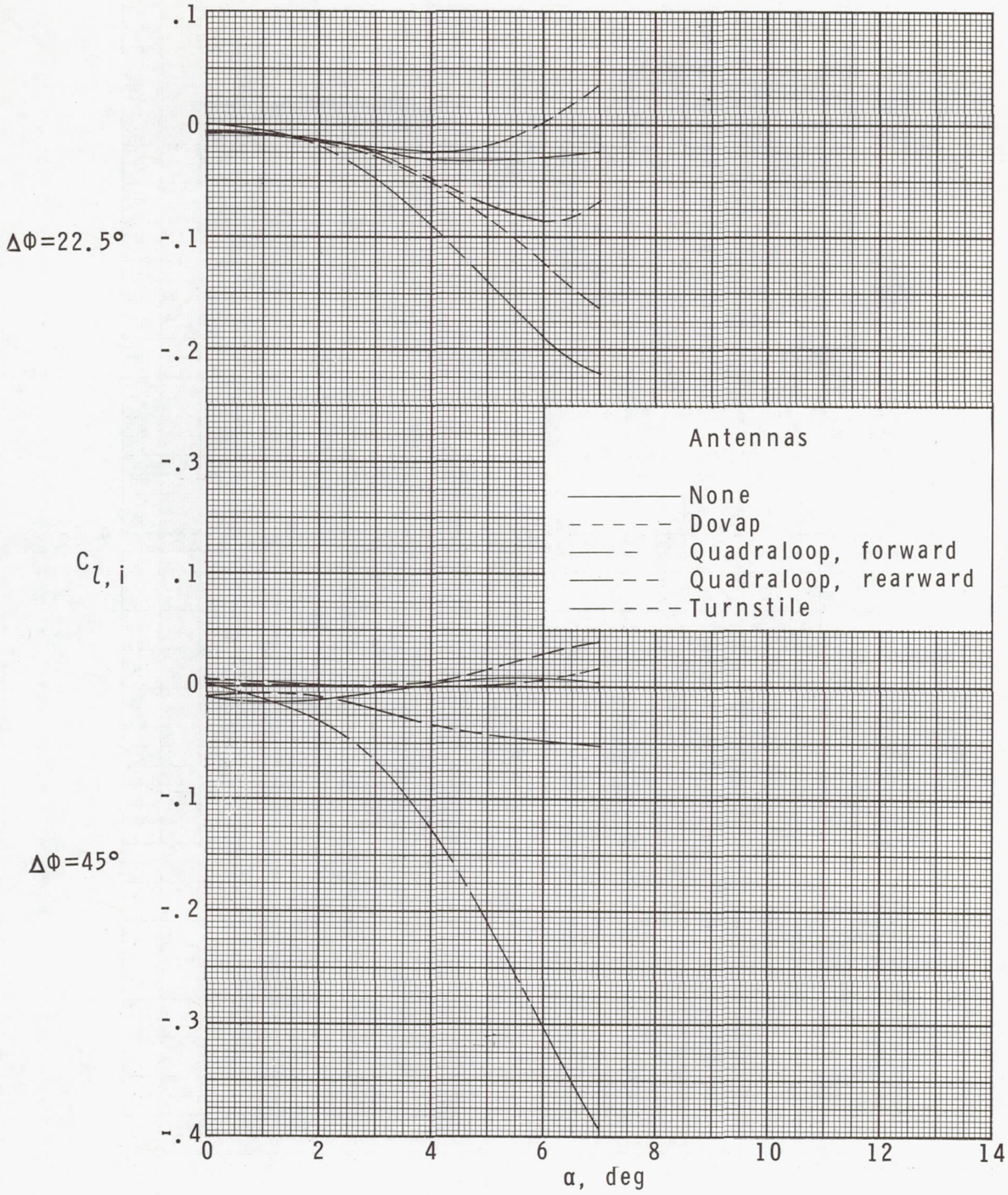

(a) M = 2.30.

Figure 14.- Variation of the induced rolling-moment coefficient with angle of attack.

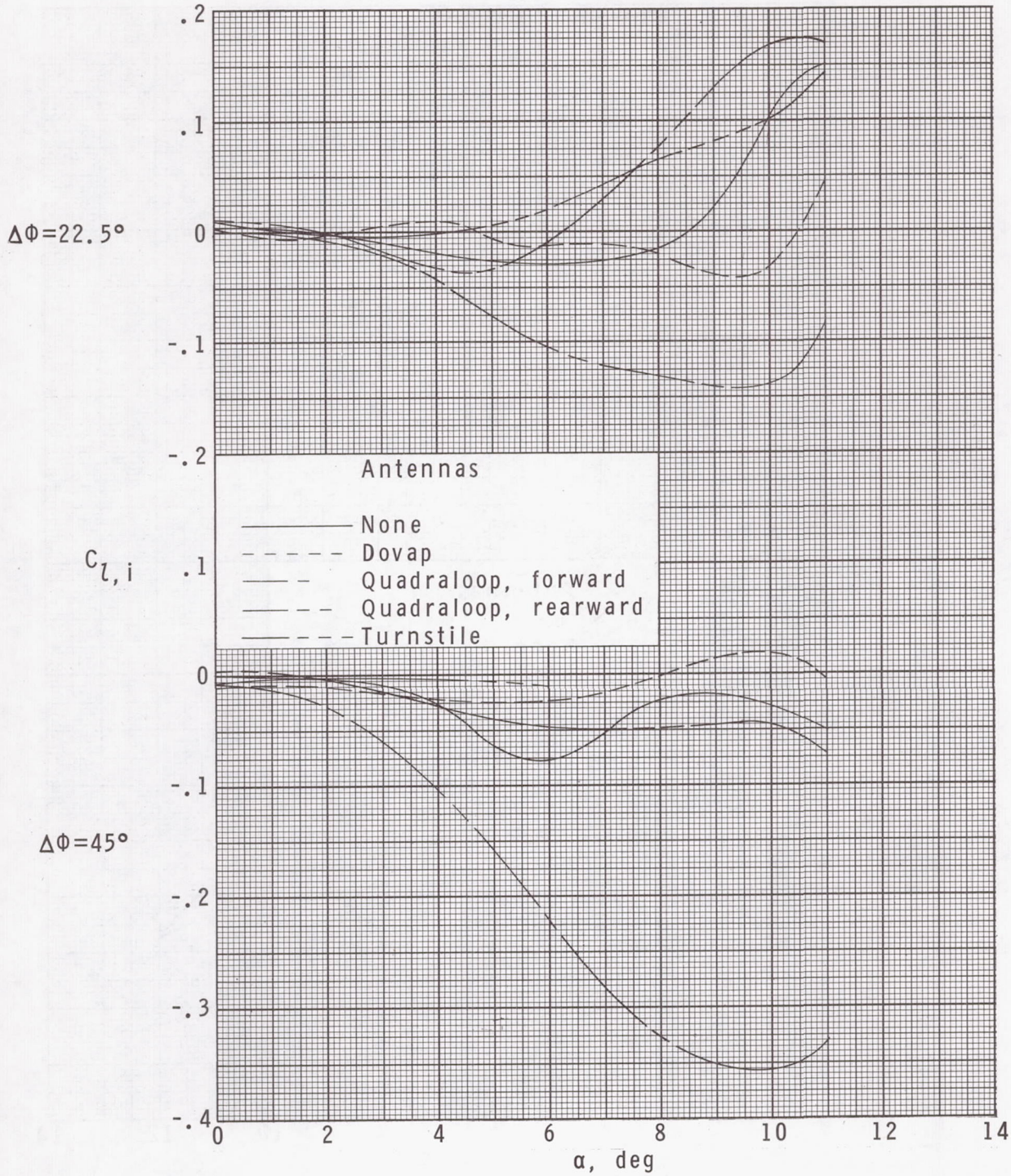

(b) M = 2.96.

Figure 14.- Continued.

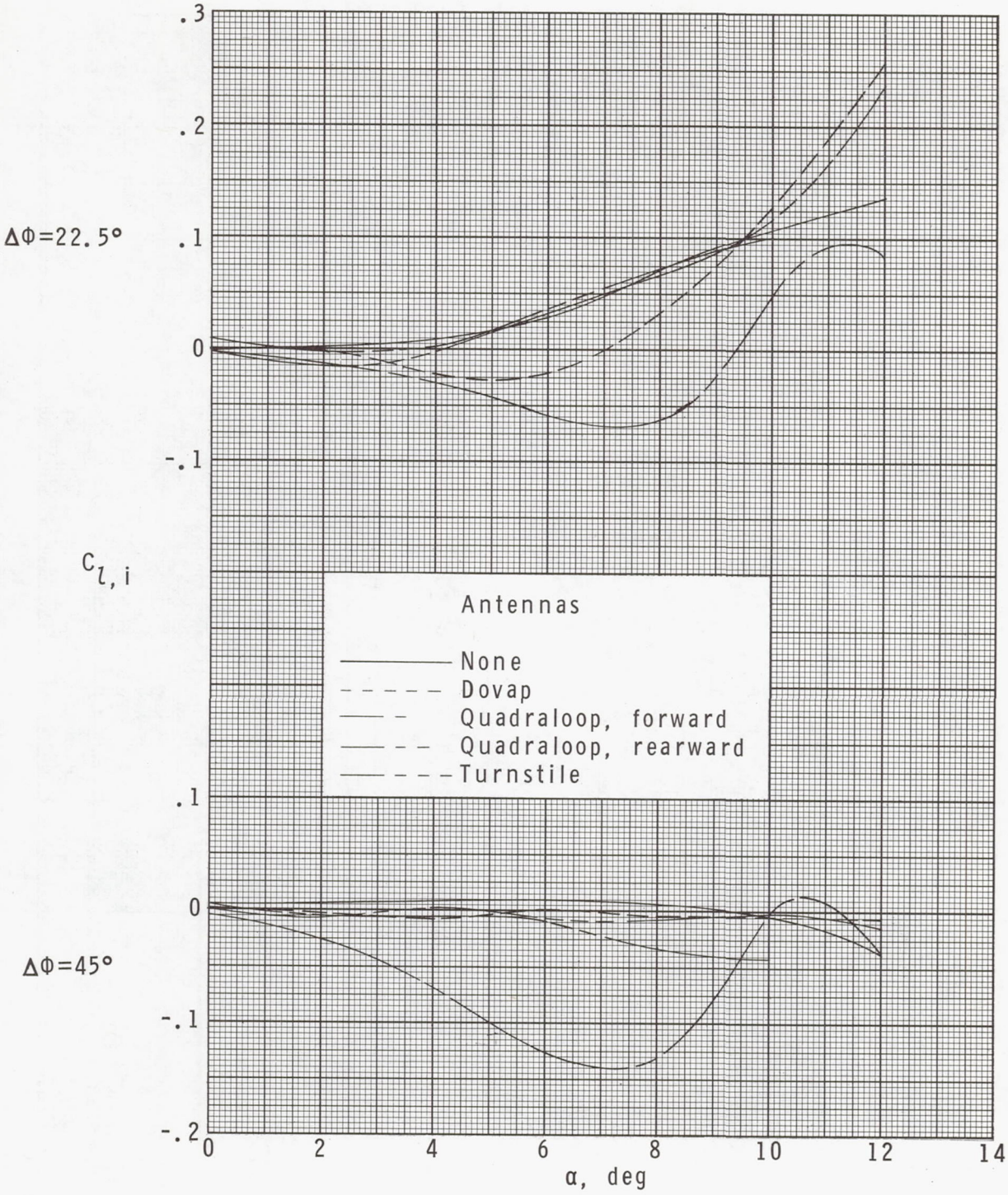

(c) M = 3.95.

Figure 14.- Continued.

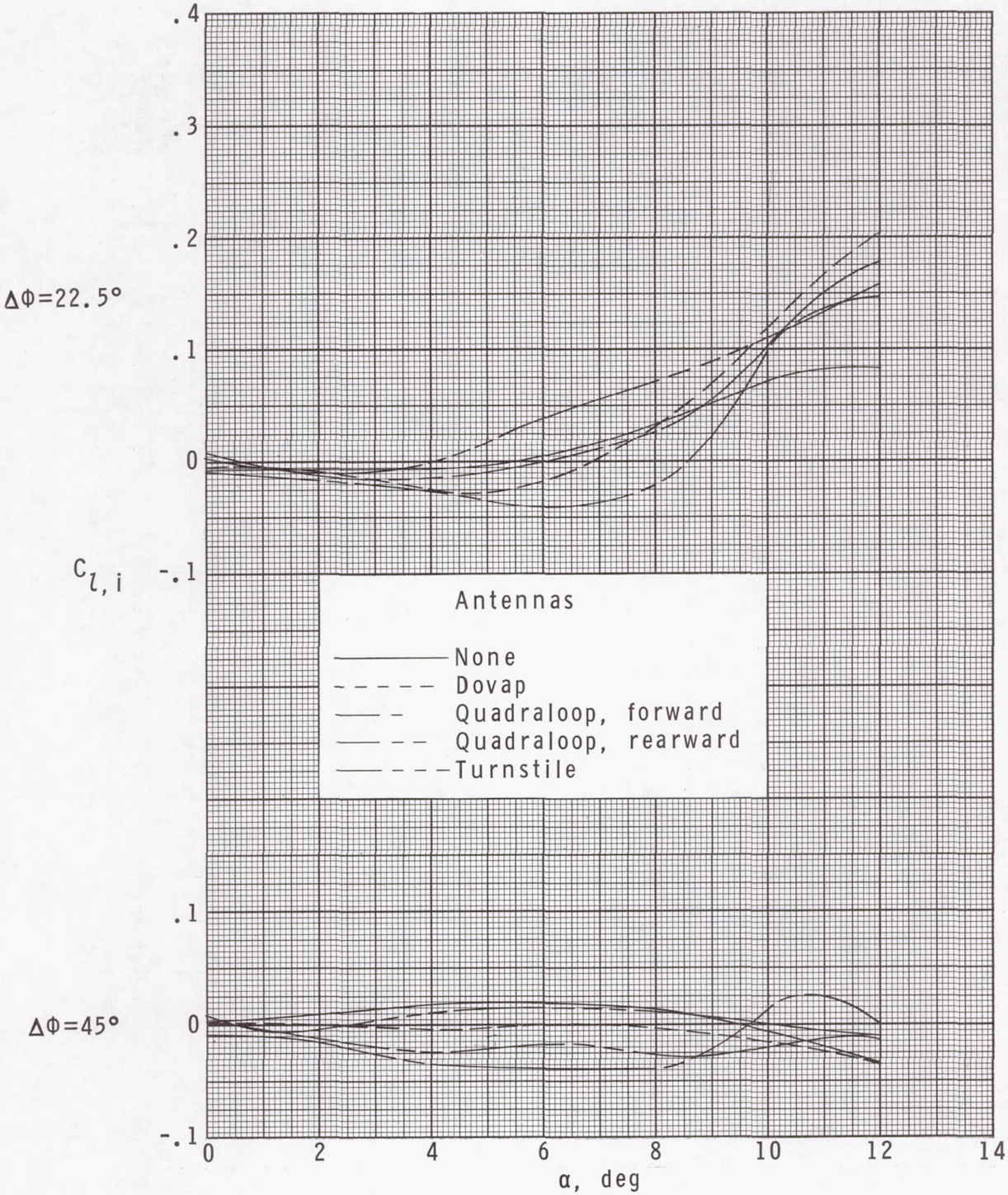

(d) M = 4.63.

Figure 14.- Concluded.

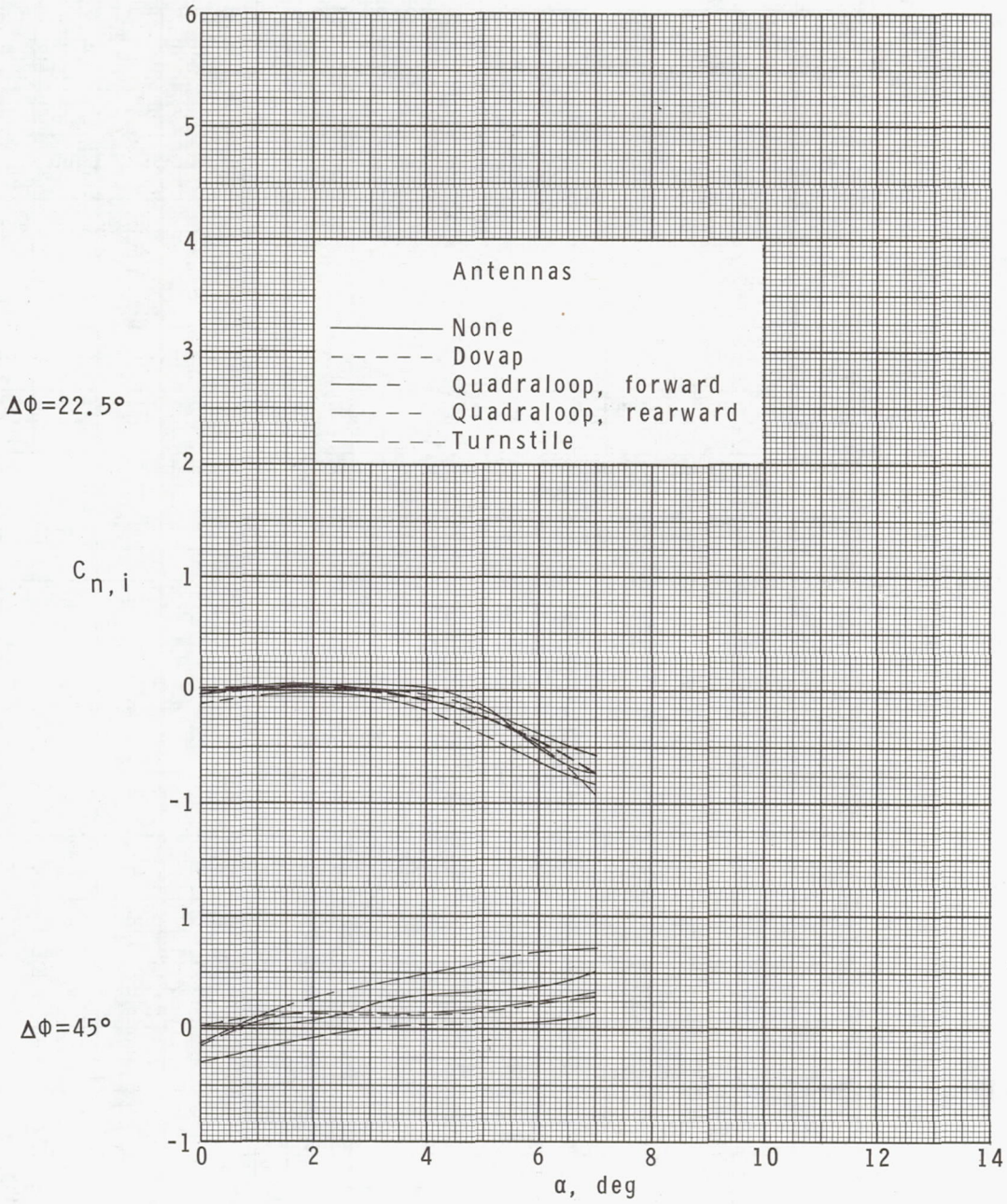

(a) M = 2.30.

Figure 15.- Variation of induced yawing-moment coefficient with angle of attack.

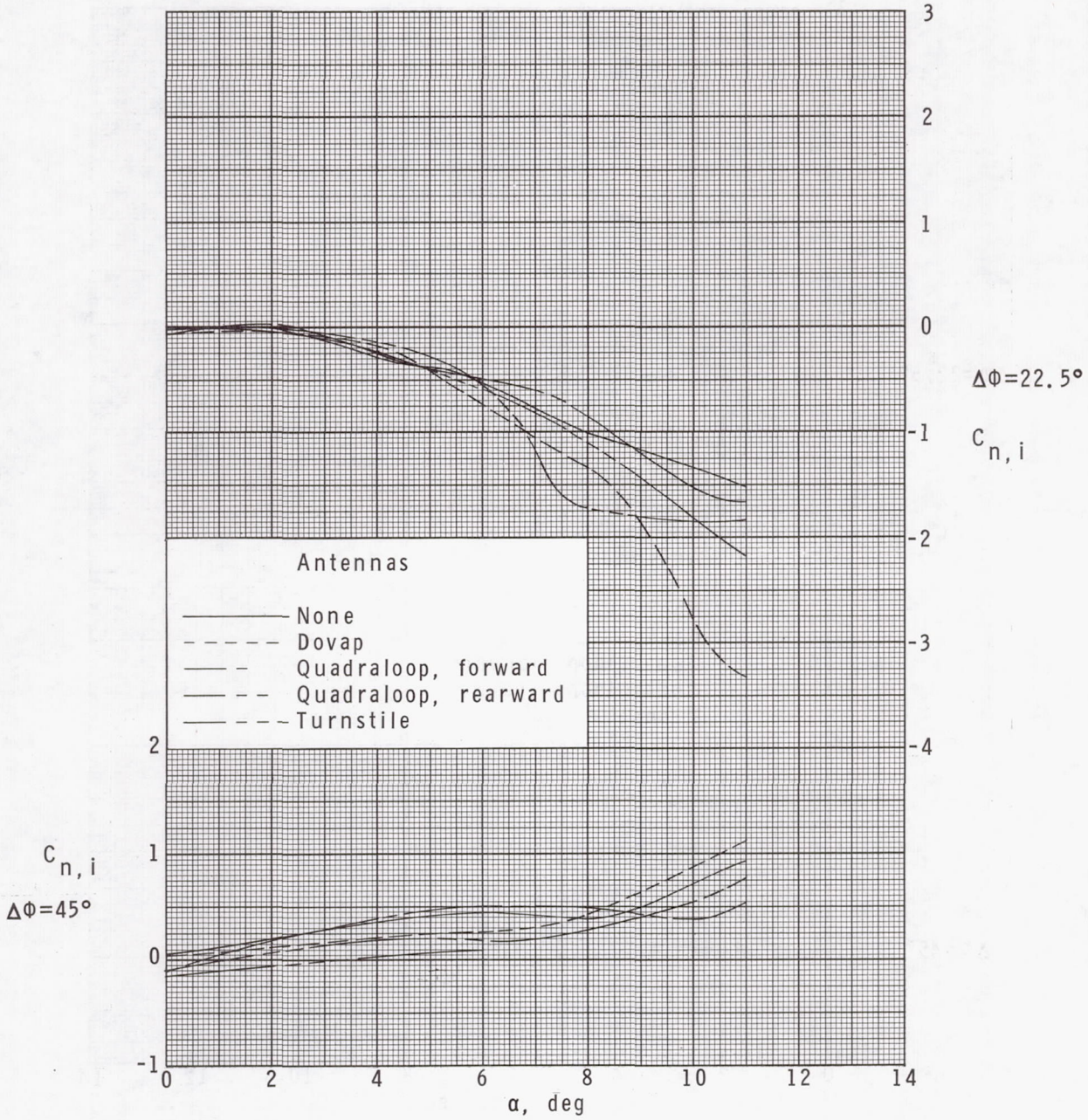

(b) M = 2.96.

Figure 15.- Continued.

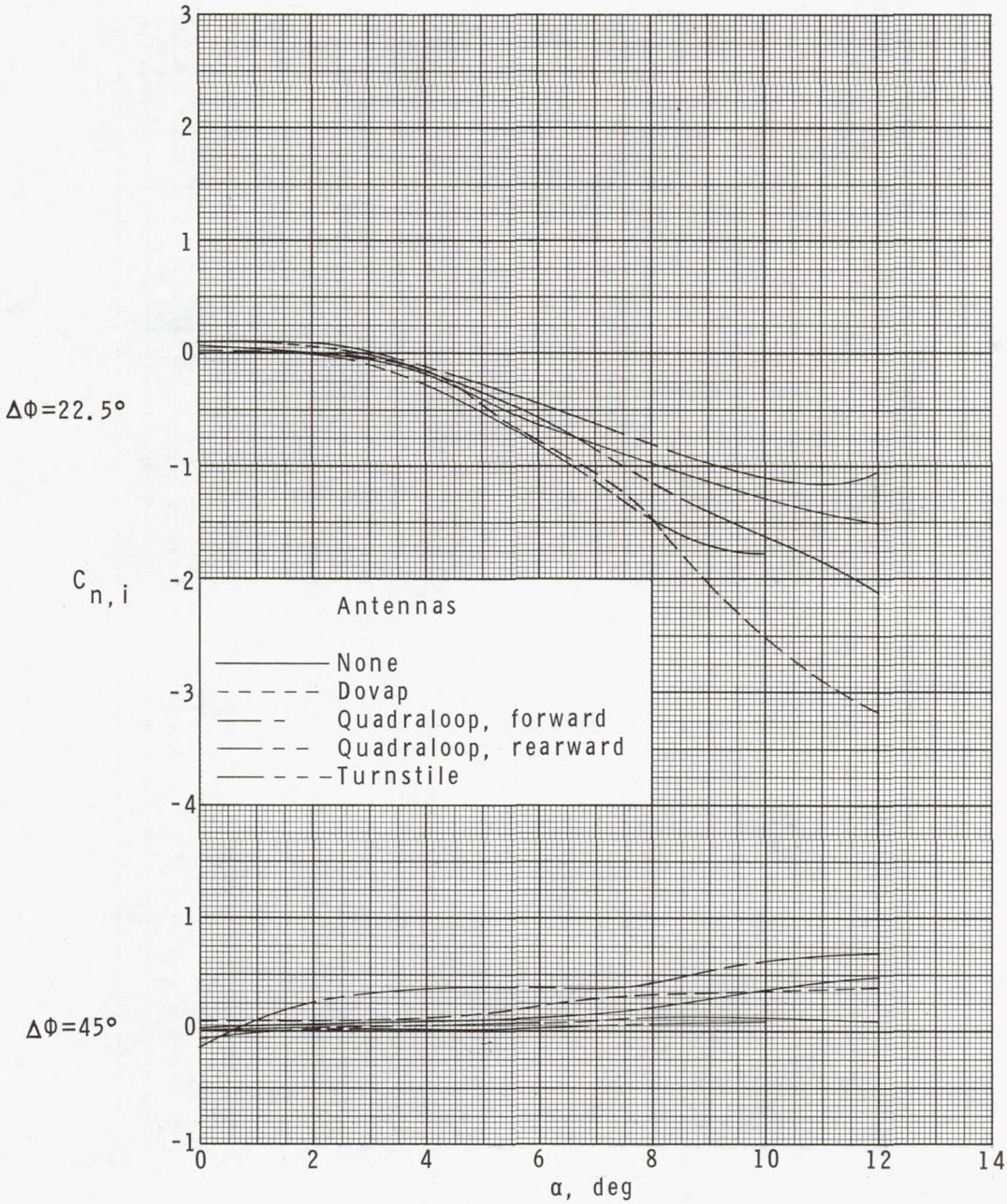

(c) M = 3.95.

Figure 15.- Continued.

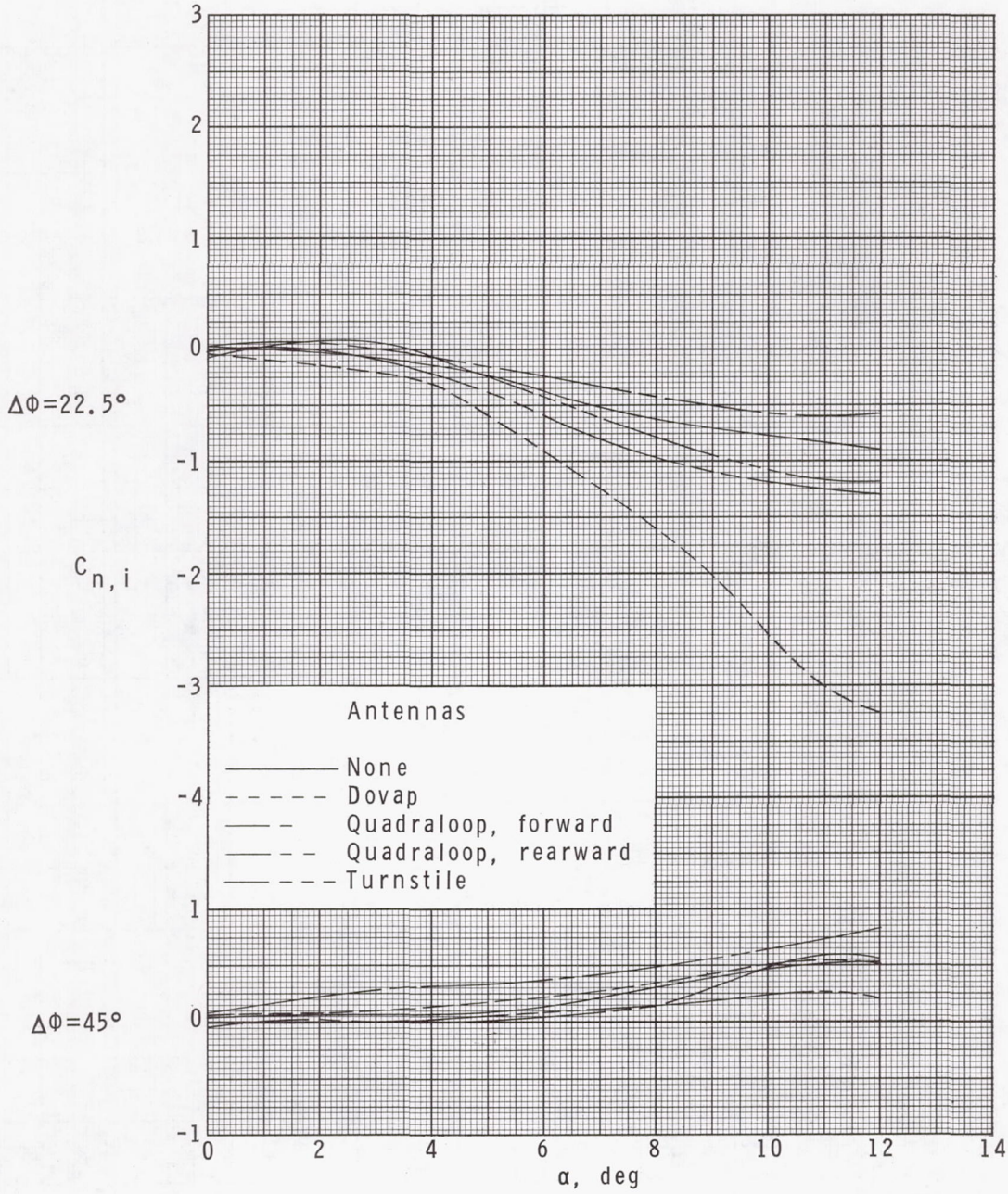

(d) M = 4.63.

Figure 15.- Concluded.

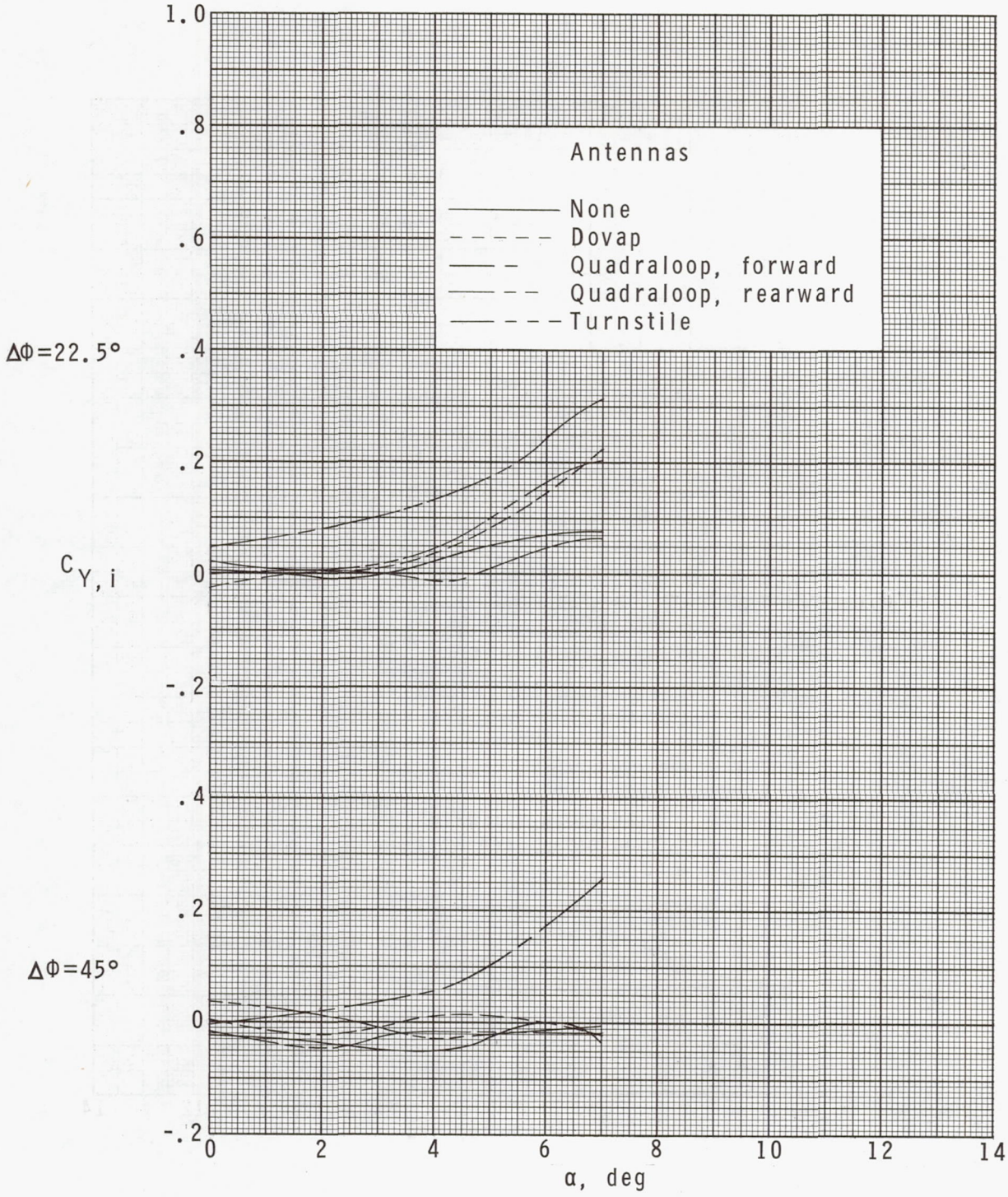

(a) M = 2.30.

Figure 16.- Variation of induced side-force coefficient with angle of attack.

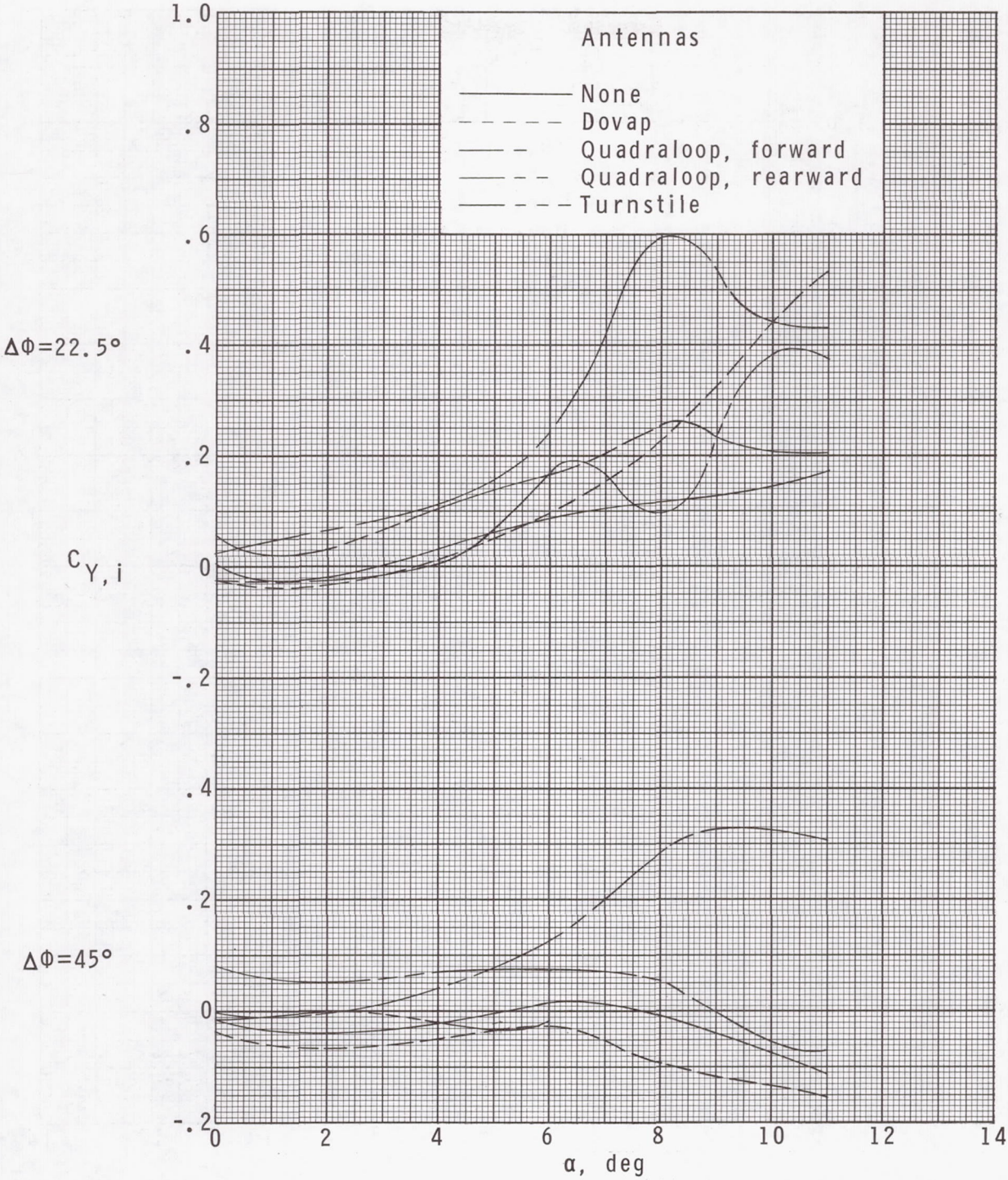

(b) M = 2.96.

Figure 16.- Continued.

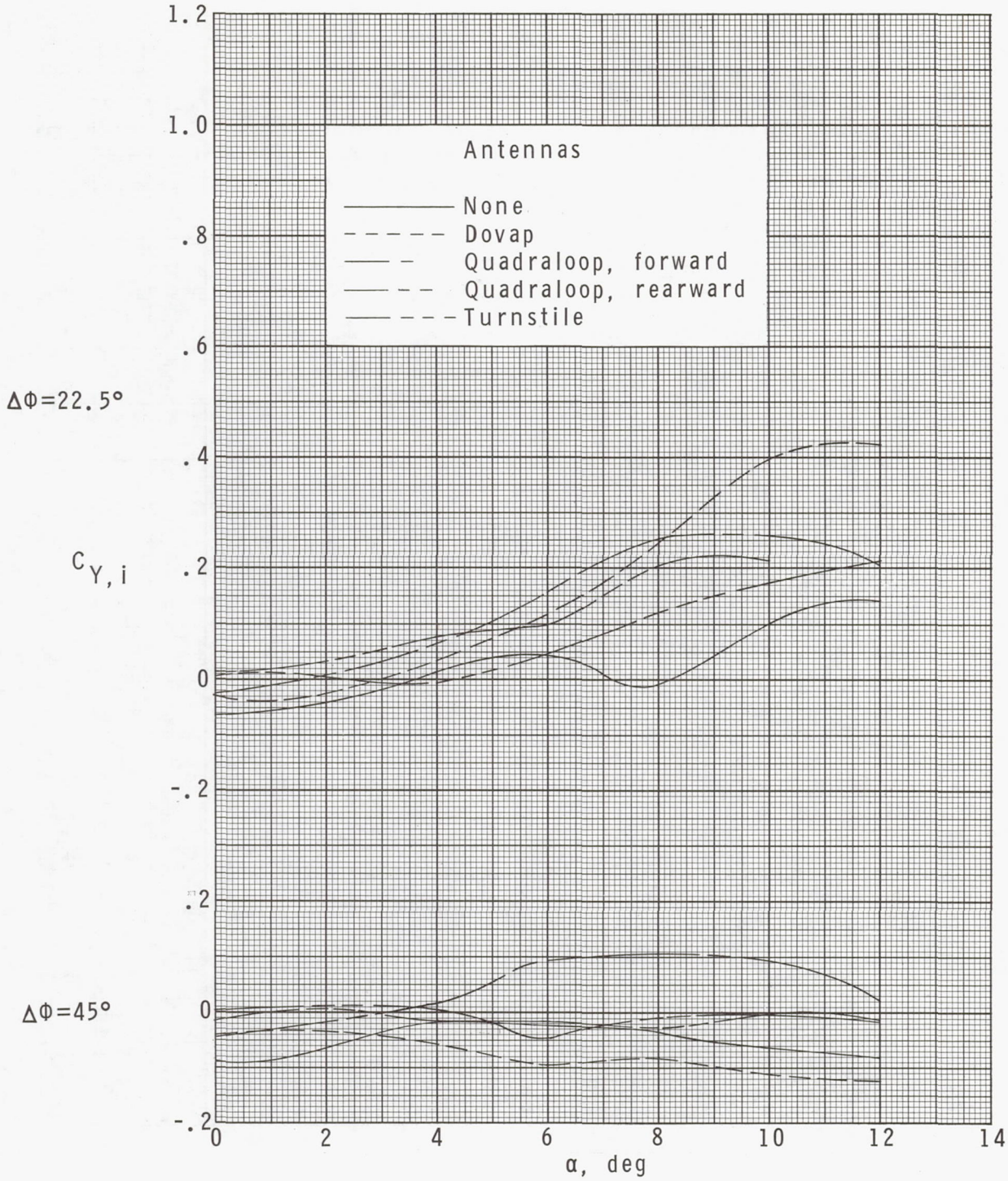

(c) M = 3.95.

Figure 16.- Continued.

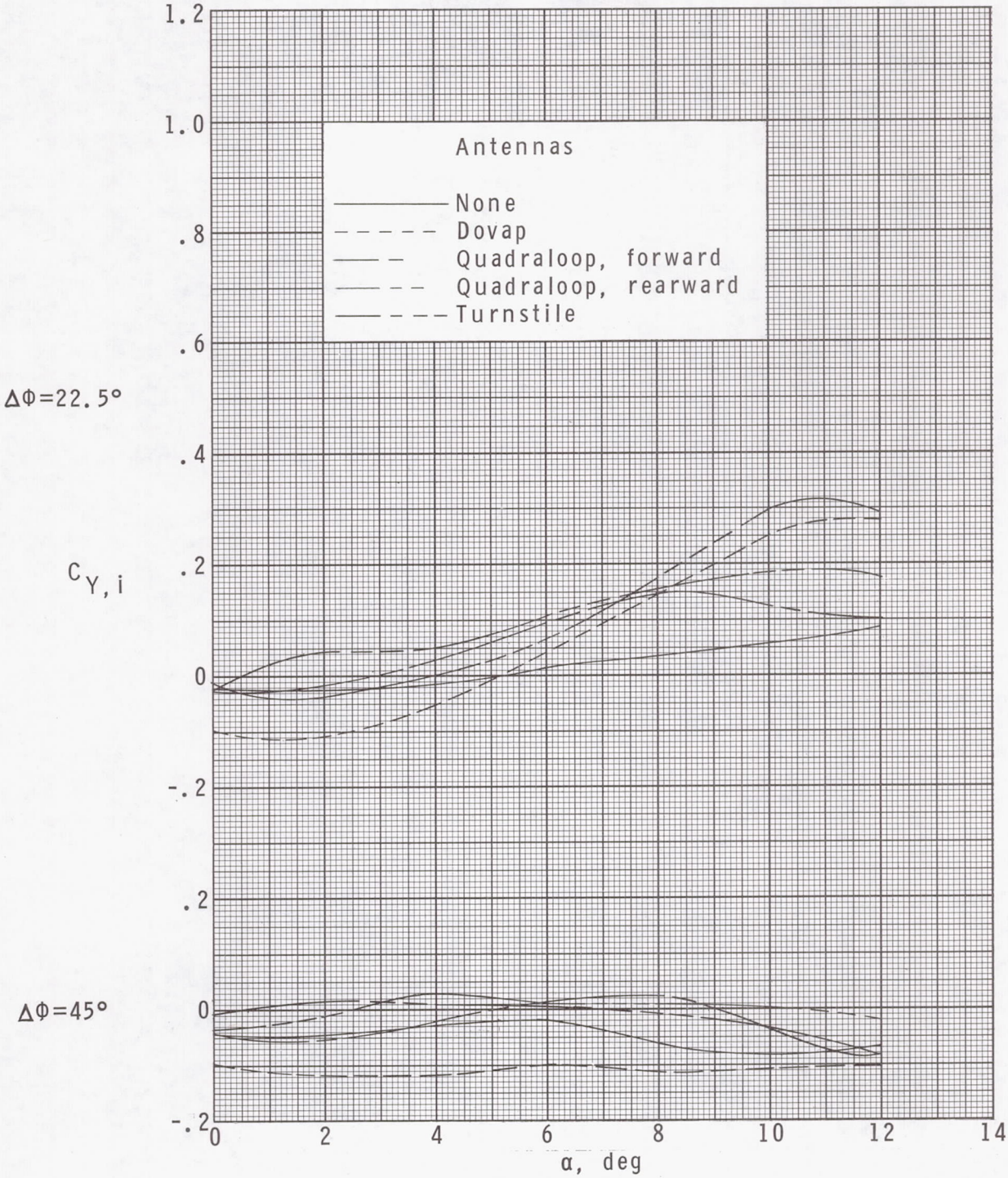

(d) M = 4.63.

Figure 16.- Concluded.